remote sensing

MDPI

Article

Glacier Volume Changes Across the Greater Caucasus Between 1960 and 2025

Levan G. Tielidze [1,2,*], Yingkui Li [3], Roman M. Kumladze [2,4], Weilin Yang [1] and Andrew N. Mackintosh [1]

[1] School of Earth, Atmosphere and Environment, Monash University, Clayton, VIC 3800, Australia
[2] Glaciology Research Centre, School of Natural Sciences and Medicine, Ilia State University, 0179 Tbilisi, Georgia
[3] Department of Geography and Sustainability, University of Tennessee, Knoxville, TN 37996, USA
[4] National Environmental Agency, Ministry of Environment Protection and Agriculture of Georgia, 0102 Tbilisi, Georgia
* Correspondence: tielidzelevan@gmail.com

Highlights

What are the main findings?

- Glacier ice volume across the Greater Caucasus declined by 51.6%, from 88.08 ± 4.5 km^3 in 1960 to 42.66 ± 1.1 km^3 in 2025.
- Volume loss accelerated after 2000, with the largest regional decline occurring during 2014–2025; substantial spatial differences were also observed among countries and sectors.

What are the implications of the main findings?

- Glacier volume provides a more comprehensive measure of cryospheric change than glacier area alone, capturing widespread ice thinning that is not reflected by changes in glacier extent.
- The regional volume-loss record provides a quantitative baseline for assessing future glacier change, freshwater availability, and glacier-related hazards in the Greater Caucasus.

Abstract

Mountain glaciers are sensitive indicators of climate change and provide essential freshwater resources for downstream ecosystems and human societies. Although glacier area changes have been extensively investigated in the Greater Caucasus, no long-term assessments of regional glacier ice volume reconstruction have been made. This study presents the first comprehensive reconstruction of glacier ice volume changes across the entire Greater Caucasus over the past 65 years, integrating glacier inventories at five observational periods (1960, 1986, 2000, 2014, and 2025) with the automated PalaeoIce reconstruction framework. Total glacier ice volume declined from 88.08 ± 4.5 km^3 in 1960 to 42.66 ± 1.1 km^3 in 2025, corresponding to an overall loss of more than half of the Caucasus glacier volume (51.6%) since 1960. Ice volume loss accelerated markedly after 2000, with the most rapid decline (27% or −2.45 yr^{-1}) occurring between 2014 and 2025. Spatial patterns in ice volume change show pronounced regional variability. Relative ice loss over the past 65 years was greatest among glaciers in Azerbaijan, which experienced a 98.4% reduction in ice volume. In comparison, glaciers in Georgia and Russia lost 52.6% and 50.9% of their ice volume, respectively, over the same period. Sectoral analysis further reveals contrasting spatial responses across the Greater Caucasus, with the eastern sector experiencing the greatest proportional ice loss of 71.6% over the 65-year study period, followed by the western sector

Check for updates

Academic Editor: Ulrich Kamp

Received: 12 September 2026
Revised: 4 October 2026
Accepted: 15 October 2026
Published: 20 October 2026

Copyright: © 2026 by the authors. Licensee MDPI, Basel, Switzerland. This article is an open access article distributed under the terms and conditions of the Creative Commons Attribution (CC BY) license.

with 60.4% and the central sector with 47.3%. Glacier thickness also declined across the Greater Caucasus over the 65-year study period. Mean glacier thickness decreased from 28.2 ± 1.41 m in 1960 to 17.4 ± 0.75 m in 2025, while mean maximum thickness declined from 88.7 ± 4.44 m to 54.1 ± 2.33 m over the same period. These findings provide region-wide quantification of long-term glacier ice volume and thickness evolution in the Greater Caucasus and establish an important baseline for assessing glacier response to ongoing climate change, future water availability, natural hazards, and regional cryospheric evolution.

Keywords: glacier volume; Greater Caucasus; glacier change; PalaeoIce; glacier thickness

1. Introduction

Mountain glaciers are sensitive indicators of climatic variability because their mass and geometry respond to changes in temperature and precipitation over annual to decadal timescales [1–4]. Their changes affect freshwater storage, seasonal runoff, and glacier-related hazards, making quantitative assessments of glacier evolution relevant to both cryospheric science and regional water-resource management [5–7]. Glaciers worldwide have undergone widespread retreat and mass loss under sustained atmospheric warming, with losses accelerating during the twenty-first century [8–11]. Although temperature is the primary control on glacier mass balance, precipitation amount and phase, and other components affecting the glacier surface energy balance (e.g., albedo, cloud cover, wind speed, relative humidity) and climate extremes also play a role in driving glacier change [12–15].

Earth-observation data and glacier inventories have substantially improved the capacity to quantify changes in glacier area, surface elevation, and mass balance across large regions [16–19]. However, glacier ice volume remains comparatively poorly constrained because ice thickness cannot be directly mapped over extensive areas and field-based geophysical measurements are available for only a small fraction of glaciers [20,21]. Regional and global volume estimates therefore commonly rely on empirical scaling relationships, numerical flow models, inversion methods, or machine-learning approaches [22–24]. While these approaches have improved estimates of contemporary ice storage, multi-decadal reconstructions remain uncommon because they require temporally consistent glacier geometries spanning several decades [25].

Ice volume provides a more complete measure of glacier change than area alone because it captures both horizontal retreat and ice thinning. Glaciers can lose substantial thickness while undergoing relatively limited areal reduction, particularly where geometric adjustment lags climatic forcing [26]. Consequently, volume change provides a direct measure of changes in glacier ice storage and offers useful constraints for glacier evolution models and comparisons with geodetic and glaciological observations [27,28].

The Greater Caucasus is a major glacierized mountain system of western Eurasia, extending across Russia, Georgia, and Azerbaijan and containing more than 2000 glaciers. Previous studies have documented widespread glacier retreat using geochronological data, historical maps, aerial photographs, satellite imagery, and successive glacier inventories [29–36]. Glacier distribution and response vary substantially across the range because of strong longitudinal gradients in precipitation, temperature, and topography. Nevertheless, the long-term evolution of glacier ice volume across the Greater Caucasus remains poorly constrained. Recent automated ice-thickness reconstruction methods provide an opportunity to address this gap by combining historical glacier outlines with digital

elevation models and glacier flowlines to generate spatially consistent estimates of glacier thickness and volume for multiple periods [37–40].

Here, we present a comprehensive reconstruction of glacier ice volume change across the entire Greater Caucasus over the 65-year period from 1960 to 2025. We combine glacier inventories for 1960, 1986, 2000, 2014, and 2025 with the automated PalaeoIce reconstruction framework [37] to estimate glacier volume for each observation period. We then quantify temporal changes in regional ice storage and assess differences among the three countries and major physiographic sectors of the range. This approach provides a consistent regional-scale assessment of multi-decadal glacier volume evolution and its acceleration through time.

2. Study Area

The Greater Caucasus is the largest and highest mountain system in the Caucasus region, extending for approximately 1200 km between the Black Sea in the west and the Caspian Sea in the east (Figure 1). The mountain range forms a natural boundary between Eastern Europe and Western Asia and stretches across southern Russia, northern Georgia, and northwestern Azerbaijan. The range is characterized by a complex topography consisting of high mountain ridges, deeply incised valleys, extensive cirques, and numerous glacial landforms. Elevations increase from west to east-central parts of the range, where several summits exceed 5000 m above sea level (a.s.l.), including Mount Elbrus (5642 m a.s.l.), the highest peak in Europe, and Mount Kazbegi (5054 m a.s.l.).



Figure 1. The extent of modern glaciers in the Greater Caucasus. The inset map in the upper right shows the location of the Caucasus region (© Google Earth).

The hypsometric distribution of the Greater Caucasus strongly influences glacier development and preservation. Glacier accumulation areas are generally situated above 3000–3500 m a.s.l., although the equilibrium-line altitude varies considerably along the longitudinal climatic gradient. Lower equilibrium-line altitudes occur in the humid western sector owing to abundant snowfall, whereas progressively higher equilibrium-line altitudes characterize the drier eastern part of the range [41].

The Greater Caucasus is a young and tectonically active fold-and-thrust mountain belt that formed during the ongoing convergence between the Arabian and Eurasian lithospheric plates. Mountain building began during the Cenozoic and continues today, resulting in active uplift, frequent seismic activity, and rapid landscape evolution. The present-day relief reflects the interaction between tectonic uplift, fluvial erosion, glacial erosion, and hillslope processes over geological timescales [42,43].

The climate of the Greater Caucasus is controlled by the interaction of large-scale atmospheric circulation, complex mountain topography, and strong elevation-dependent climatic gradients. Moist air masses originating from in the Black Sea region dominate the western sector of the mountain range, producing abundant precipitation throughout the year. In contrast, continental air masses exert an increasing influence toward the east, where precipitation decreases substantially and seasonal temperature variability becomes more pronounced.

Air temperature decreases systematically with altitude, resulting in persistent snow cover and glacier accumulation at high elevations despite regional atmospheric warming. Mean annual temperatures range from positive values in foothill regions to well below freezing in the highest alpine environments. Seasonal contrasts are considerable, with cold, snow-rich winters followed by relatively short summers during which glacier melt reaches its annual maximum.

Annual precipitation exhibits marked spatial variability, generally exceeding 2000 mm in parts of the western Greater Caucasus while decreasing to less than 800 mm in the eastern sector. Much of the precipitation falling at high elevations occurs as snow during winter and spring, feeding glacier accumulation zones [44].

The Greater Caucasus contains one of the largest concentrations of mountain glaciers in western Eurasia and represents the principal glacierized region between the European Alps and the high mountains of Central Asia. Glacier distribution is strongly controlled by altitude, topographic shading, aspect, and regional climatic conditions. The majority of glaciers occupy north-facing slopes and deeply incised valleys where lower incoming solar radiation and favourable snow accumulation conditions promote glacier preservation [36,45,46].

3. Materials and Methods

3.1. Glacier Inventories

Five regional glacier inventories representing 1960, 1986, 2000, 2014, and 2025 [32,34,36] were compiled to provide temporally consistent glacier outlines for the Greater Caucasus. The 1960, 1986, and 2014 inventories were derived from historical topographic maps and multi-temporal satellite imagery, including Corona, Landsat 5 TM, Landsat 8 OLI, and ASTER data, with glacier margins manually delineated across the entire mountain range [32]. The 2000 inventory was subsequently developed using Landsat 7 ETM+ imagery (http://earthexplorer.usgs.gov) (accessed on 24 September 2026), following a consistent manual delineation approach to document glacier extent at the beginning of the twenty-first century [34]. The most recent 2025 inventory was generated from high-resolution (3 m) PlanetScope imagery (https://www.planet.com/explorer/) (accessed on 2 October 2026) acquired primarily during August–September 2025, supplemented by 30 m ALOS topographic data, enabling more detailed delineation of small and debris-covered glaciers [36]. Mapping uncertainties for each inventory were estimated using the buffer method, with buffer widths defined according to the spatial resolution of the satellite products used for each observation year (approximately 10–30 m). This approach accounts for positional uncertainty associated with the manual delineation of glacier margins and the spatial resolution of the source imagery. A detailed description of

the buffer-based uncertainty estimation method is provided by Tielidze and Wheate [32] and Tielidze et al. [34,36]. Together, these inventories provide a multi-temporal record of glacier geometry spanning 65 years and form the basis for reconstructing glacier ice thickness and volume for each observation period.

3.2. Reconstruction of the Ice Thickness

Ice thickness rasters corresponding to regional glacier inventory outlines were reconstructed using PalaeoIce [37], an automated paleoglacier reconstruction model based on a flowline approach [47,48], which assumes a perfect-plasticity rheology [49], in which the driving stress (τ_D) from ice weight and surface gradient is balanced by a specified basal shear stress, τ_Y [47,50].

$$\tau_D = \tau_Y = \rho g H sin\alpha = \rho g H \frac{\partial h}{\partial x} \quad (1)$$

where ρ is the ice density (~900 kg m^{-3}), g is the gravitational acceleration (9.81 m s^{-2}), H is the ice thickness, α is the ice surface gradient, h is the ice surface elevation and x is the horizontal coordinate started from the glacier terminus. This equation can be solved based on a succession of discrete steps along the flowline [48,51,52].

Equation (1) is a reasonable approximation where lateral drag is negligible, such as the interior of ice sheets and ice caps. For topographically confined glaciers, however, drag from the valley sides is an important control on ice flow, and Equation (1) alone becomes unrealistic [47,48,51]. The side-drag effect can be incorporated using a shape factor, f, representing the proportion of the driving stress that is supported by the bed [50]. This factor is related to valley cross sectional geometry and can be defined as [48,50]:

$$f = \frac{A}{HP} \quad (2)$$

where A is the cross-sectional area covered by ice, H is the ice thickness at the centerline, and P is the length of the cross-section covered by ice. The shape factor is incorporated into the flowline model by replacing τ_Y with τ_Y/f in Equation (1). For an unconfined ice sheet or ice cap, f = 1; for a valley glacier, $f < 1$ and decreases with increasing valley-side drag.

Although this simplified model neglects many processes affecting glacier dynamics, it is widely used for ice-thickness reconstruction and remains practical for large regional studies. Because basal shear stress is unknown and glaciers may not be in steady state, PalaeoIce further constrains the reconstruction using "target elevations" from known surface features, such as trimlines, lateral moraines, and glacier outlines [37]. Specifically, PalaeoIce implements an automated approach to adjust basal shear stress and derive the shape factor based on the resulting ice thickness and valley cross-sectional geometry along each step of the flowline to minimize the differences between modelled ice elevations and the "target elevations" extracted from geomorphic constraints, such as trimlines, lateral moraines, and glacier outlines:

$$\text{minimize} \sum_i \left(Z_model_i - Z_{target_i}\right)^2 \quad (3)$$

where Z_model_i and Z_target_i are the derived and target elevations, respectively, at step i along the flowline. PalaeoIce divides each flowline into segments at a specified spacing and generates cross sections perpendicular to these segments. The elevation at each intersection between a cross section and a geomorphic constraint feature is extracted as a "target elevation" for the optimization. Further details are provided in Li (2023) [37].

PalaeoIce includes a set of ArcGIS tools (ArcGIS 10.8, or ArcGIS Pro 3.0) to process flowlines, generate bare earth topography, and reconstruct the thickness and surface topography of paleoglaciers. With its user-friendly ArcGIS interface, the model can automatically

derive shape factors and optimize basal shear stress along flowlines based on topography and outline constraints for a large number of glaciers, significantly improving the efficiency of regional glacier reconstruction. It has been successfully applied to paleoglacier reconstructions around the world [38–40,53–62].

In this study, we treat each inventory as a "paleo" glacier dataset with an associated time stamp. We then use the model to reconstruct the ice thickness for each inventory at the scale of individual glacier outlines. For each time stamp, the mapped glacier outline is used as the "target elevation" to adjust the shear stress and shape factor along the flowline for the ice surface elevation and thickness reconstruction. We used the updated PalaeoIce 2.0 for the reconstruction (https://github.com/yingkui2003/PalaeoIce, accessed on 1 October 2026).

We used the Shuttle Radar Topography Mission (SRTM) DEM for the reconstruction. The SRTM DEM is a 1 arc-second (approximately 30 m at the equator) global elevation dataset collected in 2000 (USGS, https://www.usgs.gov/centers/eros/science/usgs-eros-archive-digital-elevation-shuttle-radar-topography-mission-srtm-1-arc, accessed on 1 October 2026). It provides the closest representation of ice-surface elevation for the timeframe of the RGI 7 glacier outlines (around 2000). The SRTM product we used is already void-filled. We did not apply a radar-penetration correction; C-band radar can penetrate dry snow and ice, which may bias SRTM elevations low by up to a few meters in accumulation areas. This effect is small relative to the reconstructed thickness changes but introduces systematic uncertainty. The downloaded SRTM DEM tiles were reprojected to UTM zones 37N and 38N with the WGS84 ellipsoid. The vertical datum is consistent across the SRTM DEM, its derived bed topography, and the reconstructed surfaces.

PalaeoIce requires glacier flowlines and a bare-earth topography as inputs for ice thickness reconstruction. For glacial flowlines, we used Python (version 3.12) code from the Open Global Glacier Model (OGGM) [63] (http://docs.oggm.org) to extract glacier centerlines and compute disconnected geometrical centerlines based on glacier geometry and the least-cost routing algorithm of Kienholz et al. (2014) [64], which minimizes both the total elevation gain and the distance to the glacier terminus. The centerline algorithm requires both a glacier outline and an ice-surface DEM as inputs. Because the SRTM DEM was acquired in 2000, OGGM centerlines can be generated directly for the RGI 7 outlines (around 2000; [34]), and these centerlines are distributed as one of the RGI 7 products (RGI Consortium, 2023 [65]). Centerlines are unavailable for the other years (1960, 1986, 2014, and 2025). For those years, we derived centerlines by applying the same algorithm to each year's mapped outline and the SRTM DEM, assuming that the least-cost routing algorithm can still produce reasonable centerlines even though the SRTM DEM may not fully represent glacier areas that had already melted away by 2000 or earlier glacier surfaces that were thicker than in 2000. As a result, the derived centerlines may locally deviate from the true historical flow direction. Because of this limitation, as well as the complexity of the topography and glacier outlines in the Greater Caucasus, manual checking and revision were necessary to ensure the quality of the derived centerlines for each year. These disconnected centerlines were then connected for each glacier outline of each study year using the "Connect OGGM centerlines" tool in PalaeoIce 2.0 (Figure 2).

Since centerlines were generated independently for each year from that year's mapped outline, the flowline geometry differs between years and reflects the different outline shapes and extents. Longer historical tongues are represented by centerlines that extend further down-valley, following the earlier outline. Where tributaries were connected in earlier years, they are treated as part of a single glacier polygon, and the centerline follows the main trunk, with additional flowlines where the outline geometry requires them. Where tributaries were separate, they are treated as separate glaciers. Where a glacier fragments

between years, each fragment is treated as a separate glacier polygon with its own centerline from that point onward. Glaciers that were present in earlier years but absent from the 2000 inventory are reconstructed using the earlier outline and the SRTM DEM, which serves as their bed topography because no 2000 ice thickness is subtracted in these areas, as described below.

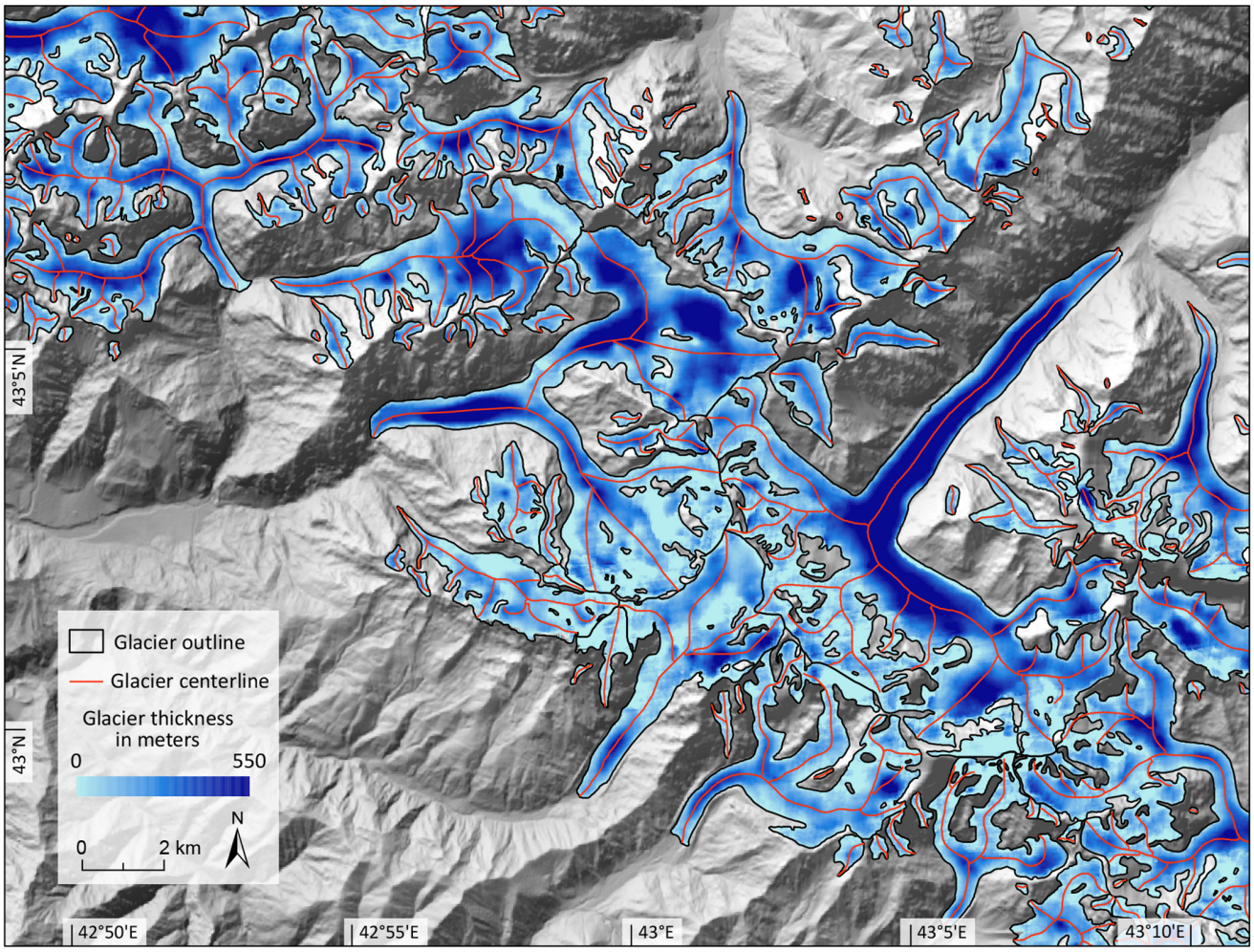


Figure 2. An example of reconstructed glacier centrelines and thickness using the SRTM DEM (~2000) and glacier outlines from 1960.

To derive a bare-earth (bed) topography for the entire region, we first used the SRTM DEM, RGI 7 glacier outlines, and connected OGGM centerlines to estimate the ice thickness for year 2000 using the "Extant Glacier Thickness (Revised From VOLTA)" tool in ArcGIS Pro 3.5. VOLTA was originally developed by James and Carrivick (2016) [66] in ArcGIS 10.1 and later revised and updated in PalaeoIce (Li, 2023) [37]. The estimated 2000 ice thickness was then subtracted from the SRTM DEM to obtain the bed topography:

$$\text{Bed topography} = \text{SRTM DEM} - \text{VOLTA thickness} \quad (4)$$

This bed topography is held fixed across all five years. The initial VOLTA-based estimate is used only once, to construct the bed. For areas that were glacier-covered in earlier years but ice-free by 2000, the bed is effectively the SRTM surface, because no 2000 ice thickness is subtracted outside the 2000 outline. We note that this bed topography may still contain glacial deposits, talus, landslides, lakes, and other erosional or depositional features, and it may also reflect paraglacial adjustment following glacier retreat (e.g., slope

debuttressing, sediment redistribution, thermokarst). However, it is difficult to quantify the thickness or magnitude of these features and processes. The bed topography is therefore a model-derived boundary condition, not an independent observation. A full sensitivity analysis with multiple bed models is beyond the scope of this study. Since absolute volume estimates carry this uncertainty, relative changes between years are more robust than absolute values.

For each year, including 2000, PalaeoIce reconstructs ice thickness from the year-specific mapped outline and the target elevations extracted from that outline, using the fixed bed as the lower boundary. The reconstruction was performed with the "PalaeoIce Reconstruction With PalaeoIce Outline(s)" tool in ArcGIS Pro 3.5, using the bare-earth DEM, glacier outlines, and their corresponding connected centerlines as inputs. PalaeoIce automatically derives the shape factor (f = 0.445–1.0) from the cross-sectional profile along the flowlines and adjusts the shear stress to best fit the input glacier outlines [37]. Minimum and maximum shear stress values of 50 kPa and 150 kPa were specified in PalaeoIce, respectively, to ensure valid shear stress in the reconstruction [37]. The 2000 volume is therefore internally consistent with the volumes reported for the other four years, allowing direct comparison across all five years.

We acknowledge that the fixed-bed assumption does not account for subglacial sediment redistribution, paraglacial adjustment, or morphometric changes between different years, and that longitudinal surface slope is therefore partly inherited from modern topographic relief rather than true historical surface hypsometry. The target-elevation constraint uses each year's mapped outline, so the reconstructed ice surface is not simply the modern surface; however, it does not recover true historical hypsometry. We therefore interpret year-to-year differences as first-order ice-thickness and volume changes under a fixed-bed assumption, rather than as exact reconstructions of historical glacier surfaces.

PalaeoIce also does not resolve non-steady-state downwasting, dead-ice detachment, or debris insulation. Because ice thickness is reconstructed independently for each year from the mapped outline and its target elevations, changes in ice thickness and volume are driven by outline changes under the fixed-bed assumption. Where glaciers thin or lose dead ice without a change in outline, or where stagnant debris-covered ice persists within the outline, our estimates may not capture the true magnitude or timing of ice loss. For glaciers where these processes are likely important, such as surge-type, debris-covered, or stagnating glaciers, the results should be treated as first-order estimates, and regional totals are more robust than individual glacier values.

3.3. Intermodal Comparison and Uncertainty

3.3.1. VOLTA and PalaeoIce Reconstructed Thickness and Volume Comparison

We first compared the VOLTA-estimated ice thickness and PalaeoIce-reconstructed thickness for the 2187 glaciers in the RGI 7 inventory around 2000 (Figure 3). The mean ice thickness values estimated by the two methods are moderately correlated (r = 0.650, Figure 3a). The relatively high scatter is expected because VOLTA estimates ice thickness primarily from ice-surface slope, with specific treatments of effective width and a minimum slope limit to define shear stress and shape factors [66], whereas PalaeoIce reconstructs ice thickness from the bed topography and outline constraints [37]. The absolute difference between the two methods varies across glacier areas (Figure 3b), with most differences clustering between 10 and 20 m. We also calculated the thickness difference between the two methods for glacier size groups (Figure 3c), reporting the root-mean-square error (RMSE), the mean absolute error (MAE), and the mean difference (PalaeoIce − VOLTA). The differences are largest for the 0.5–1.0 km^2 and 1–5 km^2 groups (RMSE = 19.5 and 19.7 m; MAE = 16.5 and 16.4 m; mean difference = 16.1 and 15.9 m), and decrease toward

larger glaciers. The difference also decreases toward the smallest glaciers (<0.5 km^2), likely because ice thickness values are small for these glaciers.

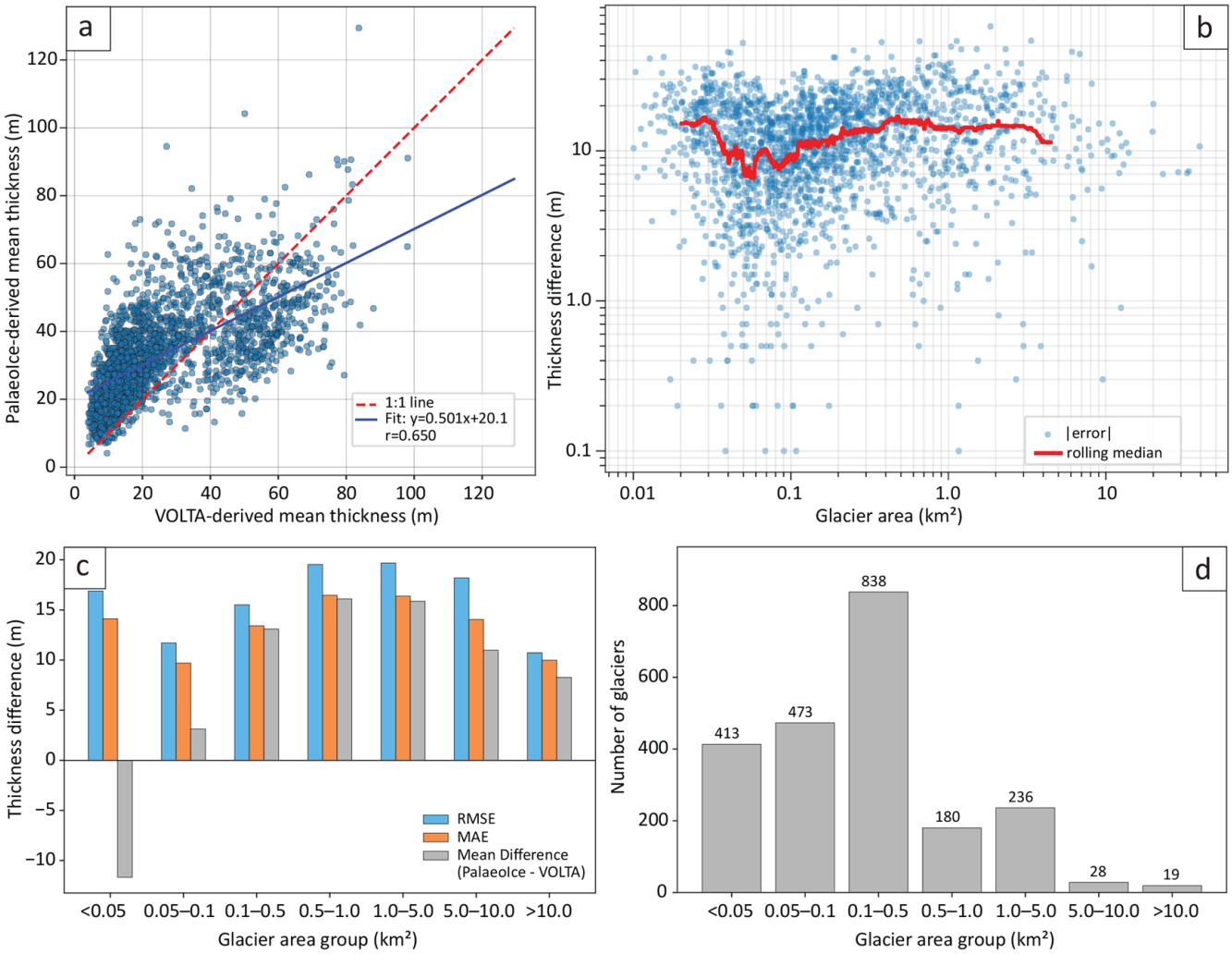


Figure 3. Comparison between the VOLTA-estimated ice thickness and PalaeoIce-reconstructed thickness for RGI 7 glacier outlines around 2000. (**a**) The correlation scatter plot between PalaeoIce reconstructed and VOLTA-reconstructed thickness. (**b**) Variations in absolute thickness difference across different glacier areas. (**c**) The RMSE, MAE, and mean difference (PalaeoIce − VOLTA) for different glacier area groups. (**d**) The number of glaciers in each area group.

Glacier areas are not normally distributed: there is a large number of small glaciers in the study area (Figure 3d), but they do not contribute significantly to the regional total ice volume, which is dominated by the large glaciers. As a result, the distribution of estimated ice volumes is also strongly skewed. Therefore, despite the relatively large scatter in ice thickness, the ice volumes estimated by the two methods are strongly correlated (Figure 4). We examined the correlation on the original volume scale and after log and cube-root transformations (Figure 4a–c). All volume correlations are very high ($r > 0.95$), with the data points clustered and the regression lines close to 1:1 line. The total ice volume estimated by VOLTA is 55.03 km^3, about 76.5% of the PalaeoIce-reconstructed volume of 71.95 km^3.

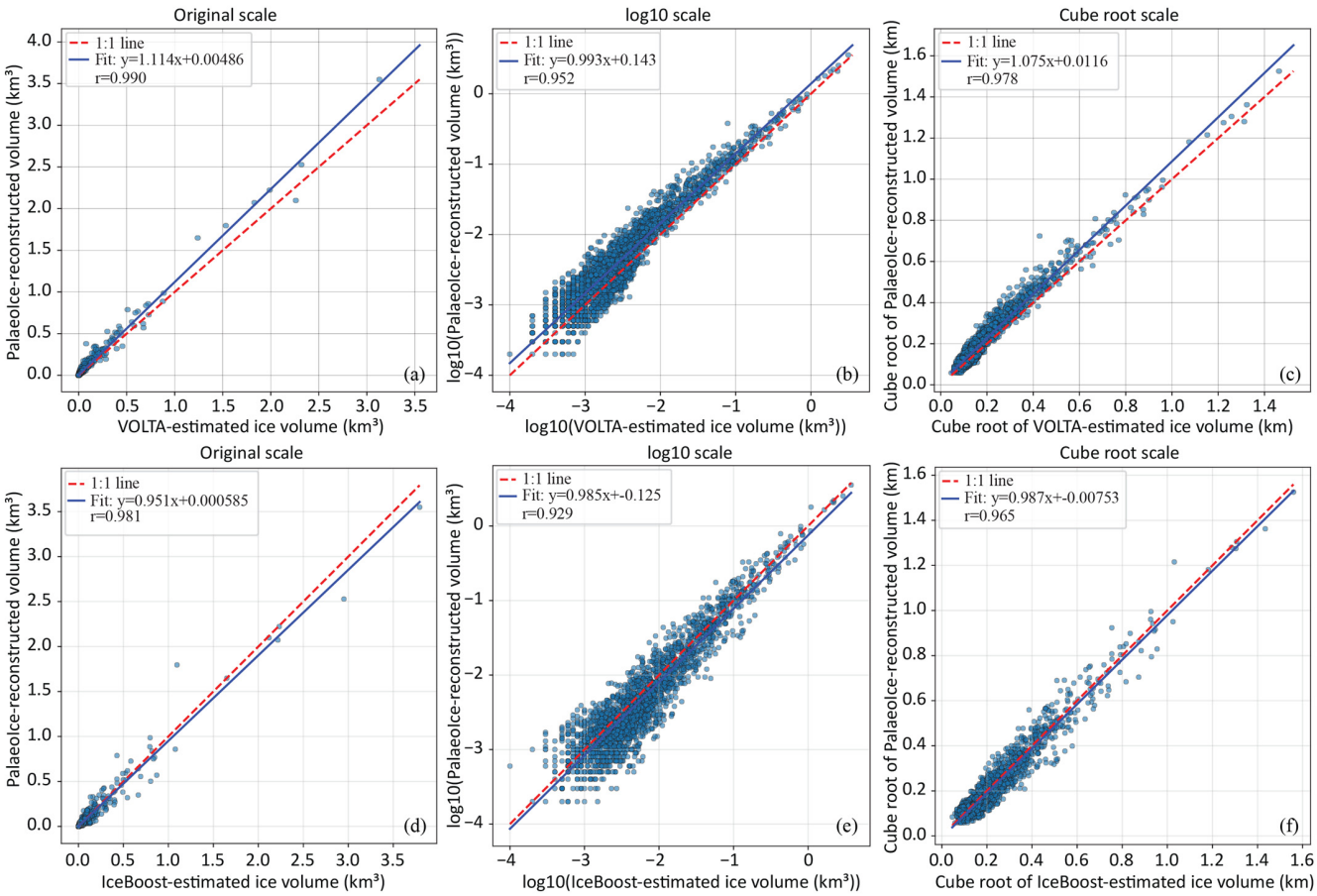


Figure 4. Scatter plots showing correlations between PalaeoIce-estimated ice volume and VOL-TA-reconstructed ice volume (**a**–**c**), and between PalaeoIce-estimated ice volume and IceBoost-derived ice volume (**d**–**f**), for RGI 7 glacier outlines around 2000. Panels (**a**,**d**) show the original scale, (**b**,**e**) the log10-transformed scale, and (**c**,**f**) the cube-root-transformed scale.

Note that this comparison is not fully independent: the VOLTA thickness estimate for 2000 is used to construct the bed topography, which is used by PalaeoIce as the lower boundary for the reconstruction. Part of the agreement between the two estimates reflects this shared dependency rather than independent methodological convergence. The comparison should be interpreted as a consistency check between the bed-topography construction input and the reconstruction output, not as an independent validation of either estimate.

3.3.2. Comparisons of PalaeoIce Reconstructed Thickness and Volume with Other Global Datasets

Although PalaeoIce-reconstructed ice thickness and volume have been validated using a few glaciers with radar-measured ice thickness data in Central Asia [37] and the southern Tibetan Plateau [67], a systematic validation for a region with a wide range of glacier types and sizes is unavailable because of the limited number of glaciers with measured ice thickness data. Furthermore, glaciers with ice thickness measurements are usually small and easily accessible, so they may not be representative of other glacier types and sizes.

Comparisons with published global glacier thickness and volume datasets provide useful context and an additional means of checking the consistency among model-estimated ice volumes. Some studies have compared regional ice volumes reconstructed using the revised VOLTA tool with the global glacier thickness and volume datasets of Farinotti et al. (2019) [68] and Millan et al. (2022) [69]. For example, the VOLTA-derived total glacier volume is about 8.7% and 5.6% less than estimates from Farinotti et al. (2019) [68]

on the southeastern Tibetan Plateau [61] and in the Tanggula Mountains of the central Tibetan Plateau [70], respectively. In the Eastern Kunlun Mountains of the northern Tibetan Plateau, Lin et al. (2026) [56] found that the VOLTA-reconstructed mean ice thickness and total volume are 13.5% and 16.9% higher than estimates from Millan et al. (2022) [69] and Farinotti et al. (2019) [68], respectively.

We compared the PalaeoIce-reconstructed ice volumes with a recently published ice volume dataset for RGI 7 glaciers based on the machine-learning approach of IceBoost ([24] https://arxiv.org/abs/2512.11685, accessed on 15 June 2026). These two estimates use the same RGI 7 glacier outlines but with very different methods: PalaeoIce is a physically based flowline model, whereas IceBoost is a machine-learning approach. Their comparison provides a cross-method consistency check. Ice volumes estimated by PalaeoIce and IceBoost are strongly correlated for individual RGI 7 glaciers, with r > 0.92 and regression slopes > 0.95 on the original volume scale and after log and cube-root transformations (Figure 4d–f). The regression lines also lie close to the 1:1 line. The total ice volume estimated by PalaeoIce (71.95 km^3) is also very close to the IceBoost-estimated total glacier volume (74.32 km^3; 3.3% difference).

The strong agreement between PalaeoIce and IceBoost for RGI 7 glaciers provides confidence in the PalaeoIce-reconstructed volumes across a wide range of glacier sizes and types, although it does not constitute independent observational validation. Since the outlines used for the other inventory years fall within a similar size and morphological range as the RGI 7 glaciers, the PalaeoIce-reconstructed volumes are expected to be reasonable for these years as well. Independent validation of the full 1960–2025 trajectory would require time-series observations of ice thickness or surface elevation change, which are not currently available for the Greater Caucasus.

In terms of uncertainty, we estimated the standard deviation of inter-model volume errors as a function of glacier area using a log-spaced rolling-window approach, which avoids the need to define discrete area bins [71]. Glaciers were sorted by $\log_{10}$(area), and for each glacier, the standard deviation of errors within the 100 nearest neighbours in log-area space was computed. A power law fitted in log-log space yields (Figure 5a):

$$\sigma(A) = 0.0207A^{0.988} (R^2 = 0.989, p < 0.001,\ n = 2187) \quad (5)$$

where $\sigma(A)$ is the standard deviation and A is the glacier area. The exponent is stable across window sizes (γ = 0.982–0.999 for k = 25–500, Figure 5b), and a non-parametric bootstrap (n = 500) yielded a 95% confidence interval of [0.953, 1.016], confirming that the estimate is robust and statistically indistinguishable from γ = 1.0 ($\sigma(A) = 0.0207A$).

Equation (5) implies an approximately constant relative uncertainty of ~2.1% (2.07%) across glacier sizes. Propagating the per-glacier σ values to the total volume under the assumption of independent errors ($\sigma_total = \sqrt{\sum \sigma_i^2}$) yields σ_total = ±2.05 km^3, or ~2.8% of the total PalaeoIce volume (71.95 km^3). The observed total volume difference between PalaeoIce and IceBoost (2.37 km^3, 3.2%) is 1.16σ, consistent with independent random errors and providing empirical support for the independent-error assumption. In contrast, the worst-case bound assuming perfectly correlated errors ($\sigma_total = \Sigma\sigma_i$) is ±28.27 km^3 (~39.3%), and the observed difference of 2.37 km^3 is only 0.08σ of that bound. We therefore adopt the independent-error estimate for the uncertainty assessment.

We applied Equation (5) to estimate per-glacier inter-model volume uncertainties for the 1960–2025 reconstructions. This extension is justified because (1) the same PalaeoIce method and bed topography were used for the ice volume reconstruction of each inventory year, and (2) glacier areas for all inventory years fall within the range of the RGI 7 glaciers used to calibrate the $\sigma(A)$ relationship (0.01–30 km^2).

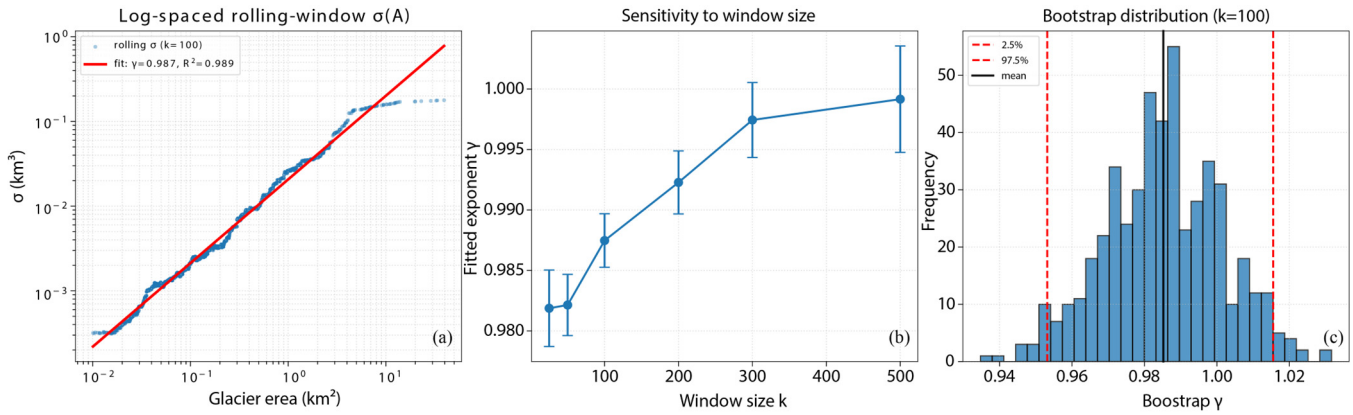


Figure 5. (**a**) Log-spaced rolling-window standard deviation $\sigma(A)$ as a function of glacier area, with the fitted power law $\sigma(A) = 0.0207A^{0.987}$ (R^2 = 0.989). The exponent is statistically indistinguishable from 1.0, indicating approximately constant relative uncertainty (~2.1%) across glacier sizes. (**b**) Sensitivity of the fitted exponent γ to the rolling-window size k. (**c**) Bootstrap distribution of γ (n = 500), with 95% confidence intervals shown as dashed red lines.

The above uncertainty assessment captures model-related uncertainty (σ_model) only, because both PalaeoIce and IceBoost used the same glacier outlines, and outline-related error therefore cancels. However, glacier outlines also contain errors related to the type and resolution of the satellite imagery used for delineation and to the experience of the investigators in identifying and digitizing outlines. Outline uncertainty (σ_outline) should therefore be added to the uncertainty assessment.

Assuming that model-related and outline-related errors are independent, the total per-glacier uncertainty can be estimated using the root-sum-of-squares (RSS) formula:

$$\sigma_i = \sqrt{(\sigma_model_i^2 + \sigma_outline_i^2)} \quad (6)$$

where σ_i, σ_model_i, and σ_outline_i are the total, model-related, and outline-related uncertainties for glacier i, respectively. This combined uncertainty is then propagated to the regional scale ($\sigma_total = \sqrt{\sum \sigma_i^2}$) under the assumption of independent errors among glaciers.

For volume differences between inventory years, we used the similar RSS formula $\sigma = \sqrt{\sigma_1^2 + \sigma_2^2}$, which assumes that errors at the two inventory years are independent. Because both inventory years share bed topography and model structure, this assumption is not strictly valid: positive covariance between epochs reduces the uncertainty in the difference. The RSS estimate therefore represents a conservative upper bound. Without a full ensemble analysis, we cannot quantify the covariance term. We note that the true uncertainty is likely smaller than the RSS estimate. We recommend that future work estimate the covariance term using ensemble or Monte Carlo methods.

Assuming that model-related uncertainty for ice volume and outline-related error for glacier area are independent of each other, we also estimated the uncertainty for the ice thickness based on:

$$\frac{\sigma_{thk}}{thk} = \sqrt{(\frac{\sigma_V}{V})^2 + (\frac{\sigma_A}{A})^2} \quad (7)$$

where $\frac{\sigma_{thk}}{thk}$, $\frac{\sigma_V}{V}$, and $\frac{\sigma_A}{A}$ are the relative uncertainties (%) of ice thickness, volume, and area, respectively.

4. Results

4.1. Regional Glacier Ice Volume Changes Between 1960 and 2025

The reconstructed glacier ice volumes reveal a substantial and continuous decline in ice storage across the Greater Caucasus during the 65-year study period (Table 1; Figure 6a). Total glacier ice volume decreased from 88.08 ± 4.4 km^3 in 1960 to 76.74 ± 4.1 km^3 in 1986, representing a reduction of ~11.34 km^3 over the first observation interval. Glacier volume continued to decline thereafter, reaching 71.95 ± 3.2 km^3 in 2000, 58.42 ± 3.1 km^3 in 2014, and 42.66 ± 1.1 km^3 in 2025. Overall, more than half of the 1960 ice volume (51.6%) has been lost (Figure 6b).

Table 1. Total glacier area and PalaeoIce-reconstructed volumes and their uncertainty for different inventory years.

Inventory Year	Area (km^2)	Area Uncertainty		Volume (km^3)	Volume Model-Based Uncertainty		Volume Combined Uncertainty	
		± km^2	± %		± km^3	± %	± km^3	± %
1960	1668.64	70.08	4.2	88.08	2.37	2.7	4.40	5.0
1986	1480.06	68.08	4.6	76.74	2.12	2.8	4.14	5.4
2000	1381.72	48.36	3.5	71.95	2.05	2.8	3.24	4.5
2014	1193.72	52.52	4.4	58.42	1.80	3.1	3.15	5.4
2025	963.91	24.09	2.5	42.66	1.51	3.5	1.09	4.3

Although glacier volume declined throughout the entire study period, the percentage ice loss was not constant. Between 1960 and 1986, glacier volume decreased by approximately 12.9%, followed by a more moderate reduction of 6.2% during 1986–2000. In contrast, glacier volume loss accelerated markedly after 2000. Between 2000 and 2014, the Greater Caucasus lost nearly one-fifth of its remaining glacier volume (18.8%), while the most pronounced reduction occurred during 2014–2025, when glacier volume decreased by an additional 27.0% (Figure 6b).

The reconstructed mean glacier thickness exhibited a contrasting temporal evolution to total ice volume. Mean thickness increased from 28.2 ± 1.41 m in 1960 to 30.4 ± 1.64 m in 1986 and 33.5 ± 1.51 m in 2000, before declining to 25.8 ± 1.39 m in 2014 and 17.4 ± 0.75 m in 2025 (Table 2). Mean maximum thickness showed a similar pattern, increasing from 88.7 ± 4.44 m in 1960 to 91.9 ± 4.96 m in 1986 and 94.6 ± 4.26 m in 2000, followed by declines to 77.4 ± 4.18 m in 2014 and 54.1 ± 2.33 m in 2025. Thus, while total glacier volume decreased continuously throughout the study period, regional mean thickness increased by 18.8% between 1960 and 2000 and subsequently declined by 47.9% between 2000 and 2025 (Figure 6a).

4.2. Spatial Variability of Glacier Ice Volume Changes Among Countries

Marked differences in glacier volume evolution were observed among the three countries that share the Greater Caucasus (Table 3; Figure 7). Throughout the study period, Russia contained the largest proportion of regional glacier ice, reflecting the extensive glacierized terrain along the northern slopes of the central and western Greater Caucasus. Glacier volume in Russia declined from 59.62 ± 3.0 km^3 in 1960 to 29.28 ± 1.3 km^3 in 2025, representing a reduction of approximately 51% over the study period.

Table 2. Mean and mean maximum glacier thickness change (m) for all Caucasus glaciers by different years according to the countries and sectors.

Year	Mean Glacier Thickness (m) According to the Countries			Mean Glacier Thickness (m) According to the Sectors		
	Russia	Georgia	Azerbaijan	Western	Central	Eastern
1960	28.64 ± 1.43	27.78 ± 1.38	21.26 ± 1.06	30.37 ± 1.52	28.28 ± 1.41	24.95 ± 1.24
1986	30.38 ± 1.64	30.51 ± 1.65	22.82 ± 1.23	31.16 ± 1.68	31.07 ± 1.68	27.02 ± 1.46
2000	33.98 ± 1.53	32.95 ± 1.48	25.53 ± 1.15	33.80 ± 1.52	34.07 ± 1.53	31.38 ± 1.41
2014	26.43 ± 1.43	25.05 ± 1.35	13.54 ± 0.73	25.47 ± 1.38	27.08 ± 1.46	21.87 ± 1.18
2025	17.89 ± 0.77	16.86 ± 0.72	6.15 ± 0.26	16.38 ± 0.70	18.51 ± 0.80	16.03 ± 0.69
Year	**Mean Maximum Glacier Thickness (m) According to the Countries**			**Mean Maximum Glacier Thickness (m) According to the Sectors**		
	Russia	**Georgia**	**Azerbaijan**	**Western**	**Central**	**Eastern**
1960	90.79 ± 4.54	85.94 ± 4.30	69.52 ± 3.48	96.31 ± 4.82	89.10 ± 4.46	76.63 ± 3.83
1986	92.89 ± 5.02	90.82 ± 4.90	71.02 ± 3.84	94.97 ± 5.13	94.57 ± 5.11	79.43 ± 4.29
2000	96.68 ± 4.35	91.77 ± 4.13	71.61 ± 3.22	95.96 ± 4.32	97.12 ± 4.37	84.92 ± 3.82
2014	79.80 ± 4.31	74.19 ± 4.01	37.88 ± 2.05	76.59 ± 4.13	81.46 ± 4.40	63.89 ± 3.45
2025	55.90 ± 2.40	51.58 ± 2.22	14.68 ± 0.63	49.34 ± 2.12	58.88 ± 2.53	47.34 ± 2.04

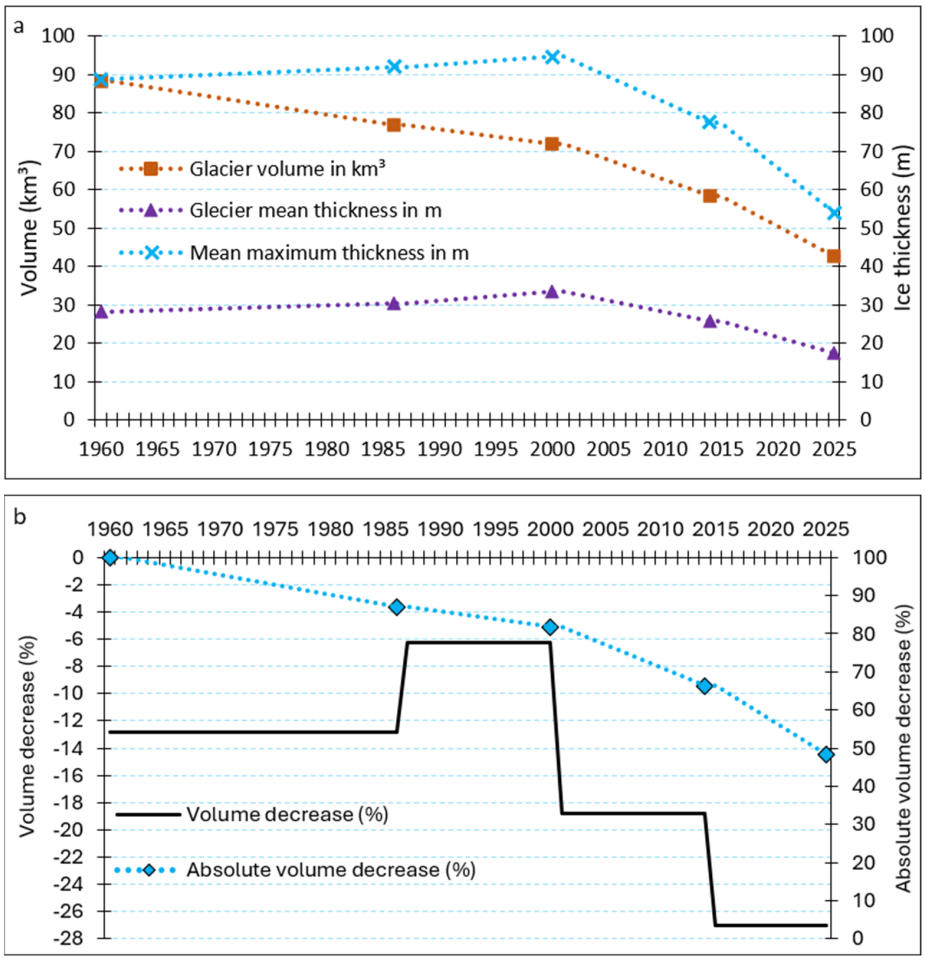


Figure 6. (**a**) Reconstructed total glacial ice volume (km^3), mean and mean maximum glacier thickness (m); (**b**) percentage and absolute percentage volume loss relative to 1960 for the entire Greater Caucasus. Data points for 1960, 1986, 2000, 2014, and 2025 are shown. The *x*-axis is scaled proportionally to time; lines between points represent linear interpolation.

Table 3. Absolute ice volume change (km^3) for all Caucasus glaciers by different years according to the countries and sectors.

Year	Absolute Ice Volume (km^3) According to the Countries			Absolute Ice Volume (km^3) According to the Sectors		
	Russia	Georgia	Azerbaijan	Western	Central	Eastern
1960	59.62 ± 2.98	28.21 ± 1.41	0.25 ± 0.0125	14.59 ± 0.73	65.81 ± 3.29	7.68 ± 0.38
1986	52.21 ± 2.82	24.36 ± 1.32	0.17 ± 0.0092	12.91 ± 0.69	58.41 ± 3.15	5.42 ± 0.29
2000	49.59 ± 2.23	22.26 ± 1.00	0.10 ± 0.0045	12.04 ± 0.54	54.63 ± 2.46	5.28 ± 0.24
2014	41.28 ± 2.23	17.13 ± 0.93	0.02 ± 0.0011	9.35 ± 0.50	45.83 ± 2.47	3.23 ± 0.17
2025	29.28 ± 1.26	13.37 ± 0.57	0.004 ± 0.0002	5.78 ± 0.25	34.69 ± 1.49	2.18 ± 0.09

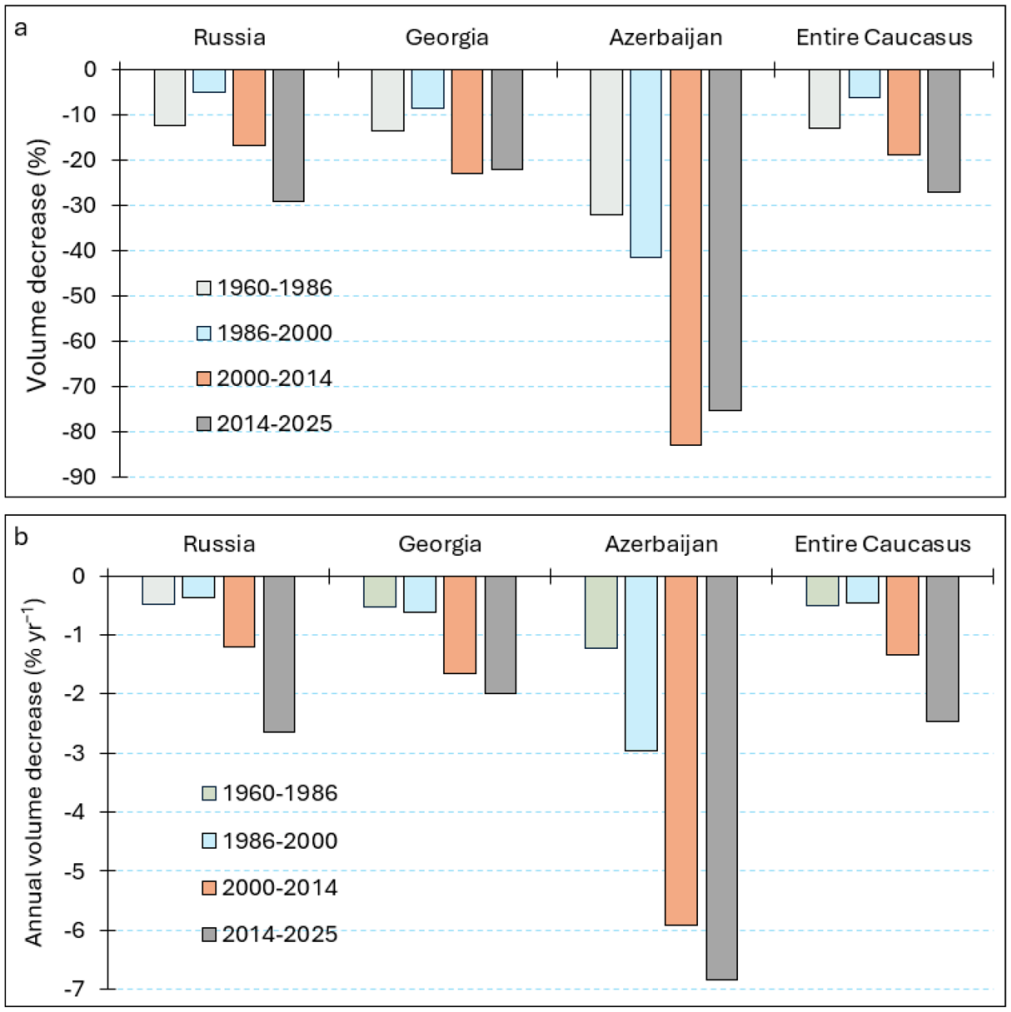


Figure 7. (**a**) Percentage and (**b**) mean annual percentage volume decrease in all Caucasus glaciers according to countries by different periods between 1960 and 2025.

Georgia, which hosts the second-largest glacierized area in the region, exhibited a similarly pronounced decline in glacier ice storage. Total glacier volume decreased from 28.21 ± 1.4 km^3 in 1960 to 13.37 ± 0.6 km^3 in 2025, corresponding to an overall loss of more than half of the ice volume. Although the absolute reduction was smaller than that observed in Russia because of the smaller initial glacier volume, the relative decrease was comparable and reflects widespread glacier recession throughout the southern slopes of the Greater Caucasus.

Glaciers in Azerbaijan contained only a small fraction of the total regional ice volume throughout the observation period, decreasing from 0.25 ± 0.0125 km^3 in 1960 to only 0.004 km^3 by 2025. Despite their limited contribution to the regional ice budget, Azerbaijani glaciers experienced by far the largest proportional losses during every observation interval, indicating exceptional sensitivity to recent climatic changes. By 2025, only a very small remnant of glacier ice remained within the Azerbaijani sector of the Greater Caucasus.

The temporal evolution of relative ice volume loss further highlights these regional differences (Figure 7a). During 1960–1986, glacier volume decreased by 12.4% in Russia, 13.6% in Georgia, and 32.0% in Azerbaijan. The differences became progressively larger during subsequent decades. Between 2000 and 2014, Azerbaijani glaciers lost 82.8% of their remaining volume, whereas glaciers in Russia and Georgia lost 16.8% and 23.1%, respectively. During the most recent period (2014–2025), glacier volume declined by 29.1% in Russia, 21.9% in Georgia, and 75.1% in Azerbaijan.

Mean annual rates of glacier volume loss show a similar temporal evolution (Figure 7b). Annual losses remained close to -0.5% yr^{-1} before 2000 for both Russia and Georgia but increased substantially thereafter, reaching -2.6% yr^{-1} in Russia and -2.0% yr^{-1} in Georgia during 2014–2025. Azerbaijan exhibited considerably higher annual rates throughout the study period, peaking at -6.8% yr^{-1} during the final observation interval. At the scale of the entire Greater Caucasus, mean annual glacier volume loss increased from approximately -0.5% yr^{-1} before 2000 to -2.5% yr^{-1} during 2014–2025, demonstrating a fivefold increase in the rate of glacier depletion over the past two decades.

4.3. Glacier Volume Changes Across Sectors

Regional subdivision of the Greater Caucasus into western, central, and eastern sectors reveals distinct spatial patterns of glacier loss (Table 3; Figure 8). The central Greater Caucasus contained the largest glacier ice reservoir throughout the study period, with reconstructed volumes decreasing from 65.81 ± 3.3 km^3 in 1960 to 34.69 ± 1.5 km^3 in 2025. The western sector experienced a reduction from 14.59 ± 0.7 km^3 to 5.78 ± 0.2 km^3, while the eastern sector exhibited the smallest glacier volumes, decreasing from 7.68 ± 0.4 km^3 in 1960 to 2.18 ± 0.09 km^3 in 2025.

The temporal evolution of percentage volume loss differed among the three sectors (Figure 8a). During the first observation period (1960–1986), the eastern Greater Caucasus experienced the greatest proportional decline (29.4%), substantially exceeding losses in both the western (11.5%) and central (11.2%) sectors. Between 1986 and 2000, glacier volume losses were relatively modest across all sectors, ranging between 2.7% and 6.7%. A pronounced acceleration occurred during 2000–2014, when glaciers in the eastern Greater Caucasus lost 38.7% of their remaining ice volume, compared with 22.3% in the western sector and 16.1% in the central sector. During the most recent observation period, however, the western Greater Caucasus exhibited the largest proportional reduction (38.2%), exceeding corresponding losses in both the eastern (32.5%) and central (24.3%) sectors.

The evolution of annual percentage volume loss further illustrates this acceleration (Figure 8b). Before 2000, annual losses generally remained below -0.5% yr^{-1} in all sectors. Between 2000 and 2014, annual volume reductions increased to -1.6% yr^{-1}, -1.2% yr^{-1}, and -2.8% yr^{-1} in the western, central, and eastern sectors, respectively. The highest annual loss rates occurred between 2014 and 2025, when glacier volume declined by -3.5% yr^{-1} in the western Greater Caucasus, -3.0% yr^{-1} in the eastern sector, and -2.2% yr^{-1} in the central sector.

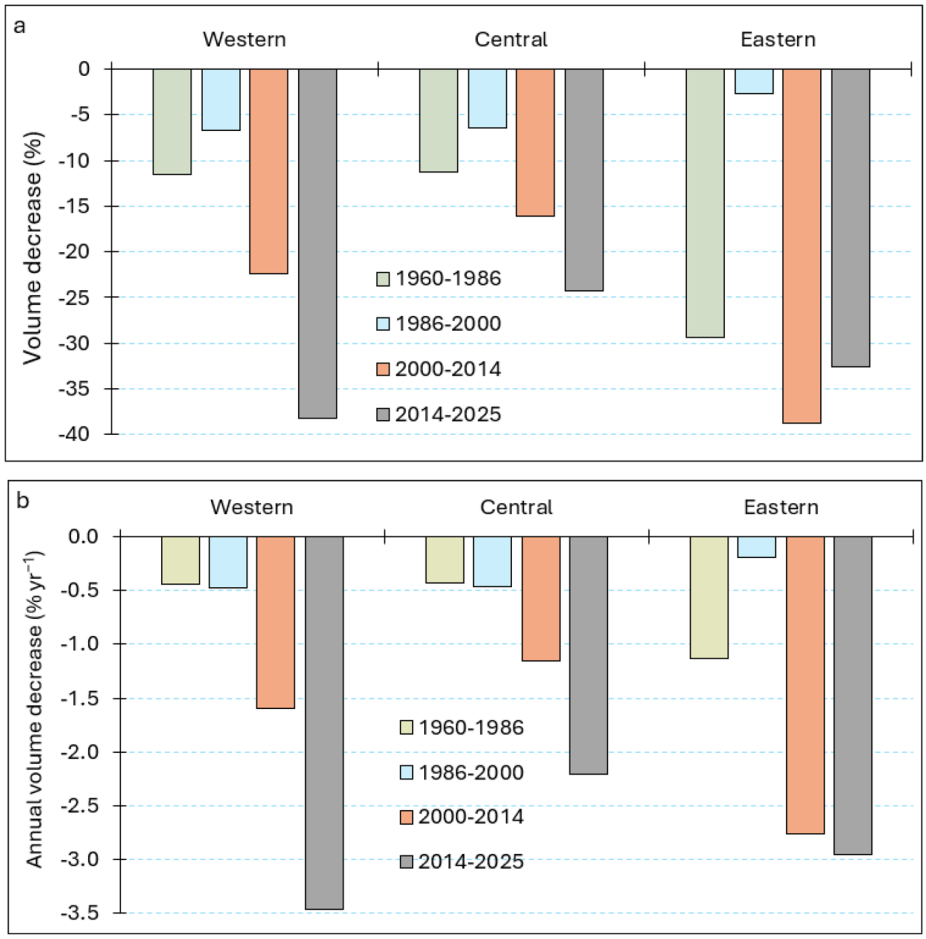


Figure 8. (**a**) Percentage and (**b**) mean annual percentage volume decrease in all Caucasus glaciers according to sectors by different periods between 1960 and 2025.

5. Discussion

5.1. Acceleration of Glacier Volume Loss Across the Greater Caucasus

The reconstructed glacier volumes demonstrate a pronounced and sustained reduction in glacier storage across the Greater Caucasus over the past 65 years, accompanied by a clear acceleration of ice loss during the twenty-first century. While glacier recession was already evident between 1960 and 2000, both the magnitude and the rate of glacier volume loss increased substantially after 2000, with the most rapid decline occurring during the most recent observation period (2014–2025). This temporal evolution closely reflects the widespread acceleration of glacier mass loss reported for mountain regions worldwide [10] and provides compelling evidence that the rate and volume change in glaciers in the Greater Caucasus is accelerating due to ongoing climatic warming.

The observed temporal acceleration of ice loss is consistent with the increasingly warmer climatic conditions that have affected the Greater Caucasus during recent decades. Instrumental meteorological observations and regional climate analyses indicate significant atmospheric warming throughout the Caucasus since the late twentieth century, accompanied by changes in precipitation phase, earlier snowmelt, prolonged ablation seasons, and increasing frequencies of exceptionally warm summers [72,73]. Together, these processes contribute to increasingly negative glacier mass balances and accelerated reductions in glacier thickness and volume.

Our results further reveal pronounced spatial variability in glacier volume loss throughout the Greater Caucasus. This contrast largely arises from differences in glacier size, altitude, and climatic setting. Azerbaijani glaciers are generally smaller (<0.01 km^2),

occupy lower total glacierized areas, and are situated near the eastern margin of the Greater Caucasus, where climatic conditions become increasingly continental and annual precipitation decreases substantially [44]. Smaller glaciers typically possess shorter response times and lower ice reserves, making them particularly vulnerable to sustained atmospheric warming [74–76]. Once persistent negative mass balance is established, such glaciers are capable of losing a very large proportion of their remaining volume within only a few decades [77].

The apparent increase in regional mean glacier thickness between 1960 and 2000, despite a continuous decline in total glacier volume, should be interpreted cautiously. Changes in glacier extent and in the population of glaciers included in the regional assessment may influence the calculated mean thickness and do not necessarily indicate actual glacier thickening. The apparent increase may also reflect methodological limitations associated with the outline-driven reconstruction and the use of fixed bed topography, which cannot fully account for historical changes in glacier geometry and hypsometry. This limitation is particularly relevant to the 1960–2000 interval because the SRTM-derived topography represents approximately the year 2000 and therefore does not directly capture historical glacier-bed geometry.

From a hydrological perspective, the observed reduction in glacier ice volume and thickness represents a substantial decline in the long-term freshwater storage of the Greater Caucasus. Continued glacier thinning will inevitably reduce the capacity of glaciers to sustain summer river discharge during dry years, potentially affecting downstream water availability for hydropower generation, irrigation, agriculture, and domestic consumption. At the same time, ongoing glacier retreat is likely to increase the formation and expansion of proglacial lakes, modify sediment transport, and alter the frequency of glacier-related hazards such as glacier collapses, debris flows and glacial lake outburst floods. Consequently, the glacier volume changes documented here extend well beyond the cryosphere itself and have important implications for regional environmental management and climate adaptation strategies.

5.2. Comparison Between Glacier Volume and Area Changes

An advantage of the present study is that it enables a direct comparison between changes in glacier volume and previously reconstructed changes in glacier area across the Greater Caucasus (Figure 9). Although both variables exhibit continuous declines throughout the study period, their temporal evolution differs substantially. Glacier area decreased progressively between 1960 and 2025, whereas glacier ice volume declined considerably more rapidly, particularly after 2000. This divergence is consistent with the different ways in which glaciers respond to sustained climatic forcing and indicates that glacier area alone does not fully capture the magnitude of ongoing glacier change.

The comparison illustrates that reductions in glacier area underestimate the total loss of glacier ice stored within the mountain range. During the initial decades of the study period, changes in glacier area and volume followed broadly similar trajectories, reflecting the relatively moderate rates of glacier retreat observed before 2000. However, the relationship became increasingly nonlinear during the twenty-first century. While glacier margins continued to retreat, the reconstructed ice thickness also declined across much of the glacier area, resulting in increasingly rapid reductions in glacier volume. However, because ice thickness is reconstructed from the mapped outline and a fixed bed topography, the reconstructed volume change is not an independent measurement of interior thinning, and part of the divergence between area and volume change may arise from the model's intrinsic geometry–volume relationship rather than from observed surface lowering alone.

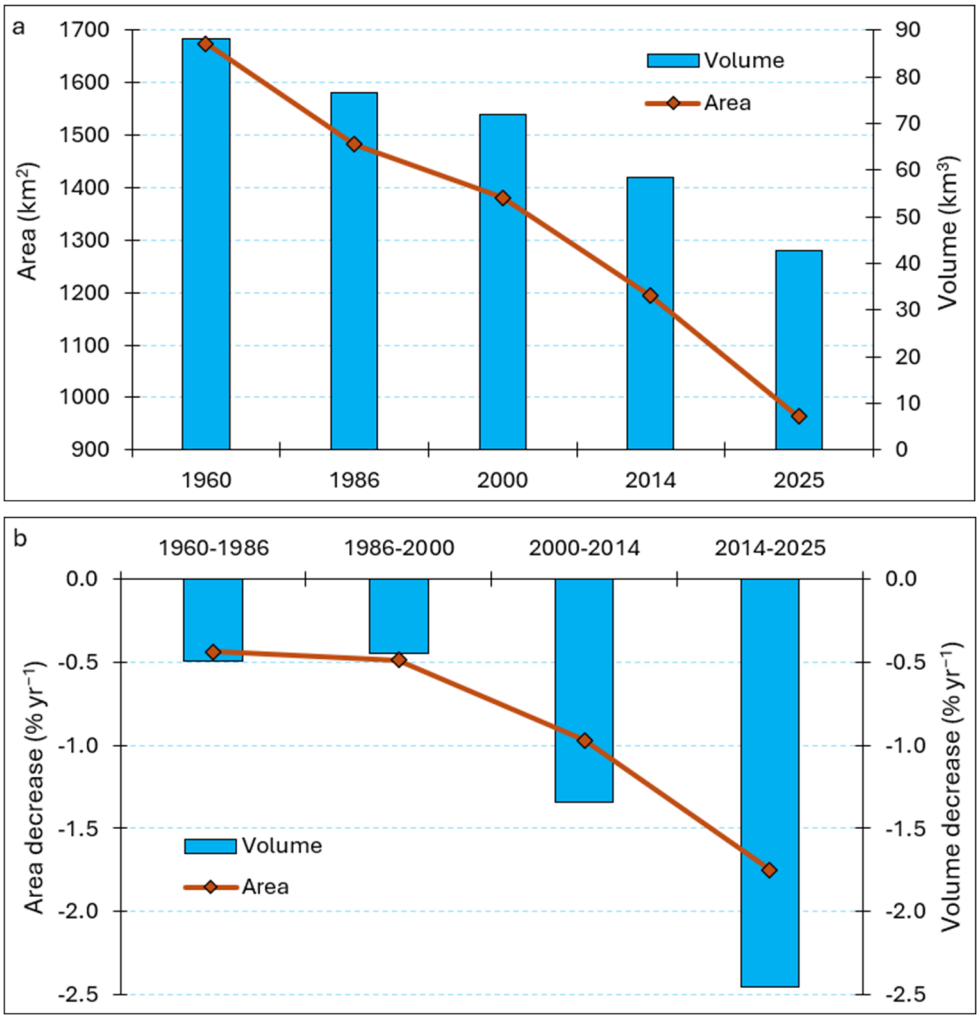


Figure 9. (**a**) Absolute ice volume (km^3) and area (km^2) decrease for all Caucasus glaciers in 1960, 1986, 2000, 2014, and 2025. (**b**) Mean annual percentage volume (km^3) and area (km^2) decrease in all Caucasus glaciers by different periods between 1960 and 2025.

Mean annual glacier area loss increased gradually throughout the observation period, whereas annual glacier volume loss accelerated much more rapidly, reaching its highest values during 2014–2025 (Figure 9b). Under the fixed-bed and outline-driven assumptions of our reconstruction, this divergence indicates that the reconstructed volume loss exceeds what would be expected from area loss alone. However, this difference should not be interpreted as direct evidence that thinning has become the dominant component of glacier change, because part of the difference arises from the model's intrinsic geometry–volume relationship and from the outline-driven construction, in which thickness change is a response to the changed outline and flowline geometry rather than an independent measurement of interior thinning. Independent observations are needed to quantify the thinning contribution to the regional signal. Similar behaviour has been documented in numerous glacierized mountain regions, where geodetic observations consistently show that reductions in glacier thickness outpace decreases in glacier extent during periods of accelerated climatic warming [8,9,78].

5.3. Comparison with Independent Glacier Volume Estimates

Local-scale estimates of glacier ice volume remain relatively scarce, making direct comparisons among studies difficult. An important exception is the study of Kutuzov et al. (2019) [33], which quantified changes in the Elbrus glacier system using extensive

ground- and helicopter-borne GPR measurements, high-resolution imagery, and digital elevation models. For Elbrus, Kutuzov et al. (2019) [33] estimated a total glacier volume of 6.52 ± 0.85 km^3 in 1997 and 5.03 ± 0.85 km^3 in 2017, compared with 6.98 ± 0.70 km^3 in 2000 and 6.54 ± 0.65 km^3 in 2014 in our reconstruction (Table 4). The difference between the estimates is therefore expected to reflect, at least in part, the different observation dates, glacier outlines, and ice-thickness reconstruction methods. In particular, the 2000 estimate in this study is approximately 6.5% higher than the 1997 estimate of Kutuzov et al. (2019) [33], whereas the 2014 estimate is approximately 23.1% higher than their 2017 estimate. These differences should not be interpreted as direct methodological biases because the corresponding observation years differ by 3 and 3 years, respectively.

Table 4. Comparison of glacier volume, area, and mean ice thickness estimates between Kutuzov et al. (2019) [33] and this study for the Elbrus glacier system.

Glacier Parameter	Kutuzov et al., 2019 [33].		Current Estimate	
	1997	2017	2000	2014
Glacier volume km^3	6.52 ± 0.85	5.03 ± 0.85	6.98 ± 0.31	6.54 ± 0.35
Mean ice thickness (m)	-	44.9 ± 7.3	45.95	40.49
Glacier area (km^2)	125.76 ± 0.65	112.20 ± 0.58	119.95± 2.34	114.53 ± 2.03

The comparison of glacier area provides additional context. Kutuzov et al. (2019) [33] reported a decrease in glacierized area from 125.76 ± 0.65 km^2 in 1997 to 112.20 ± 0.58 km^2 in 2017, while our reconstruction gives 119.95 ± 2.34 km^2 in 2000 and 114.53 ± 2.03 km^2 in 2014. Thus, the two datasets produce broadly comparable glacier extents and show the same direction of change. Similarly, Kutuzov et al. (2019) [33] reported a mean ice thickness of 44.9 ± 7.3 m in 2017, compared with 45.95 ± 4.6 m in 2000 and 40.49 ± 4.5 m in 2014 in our reconstruction (Figure 10).

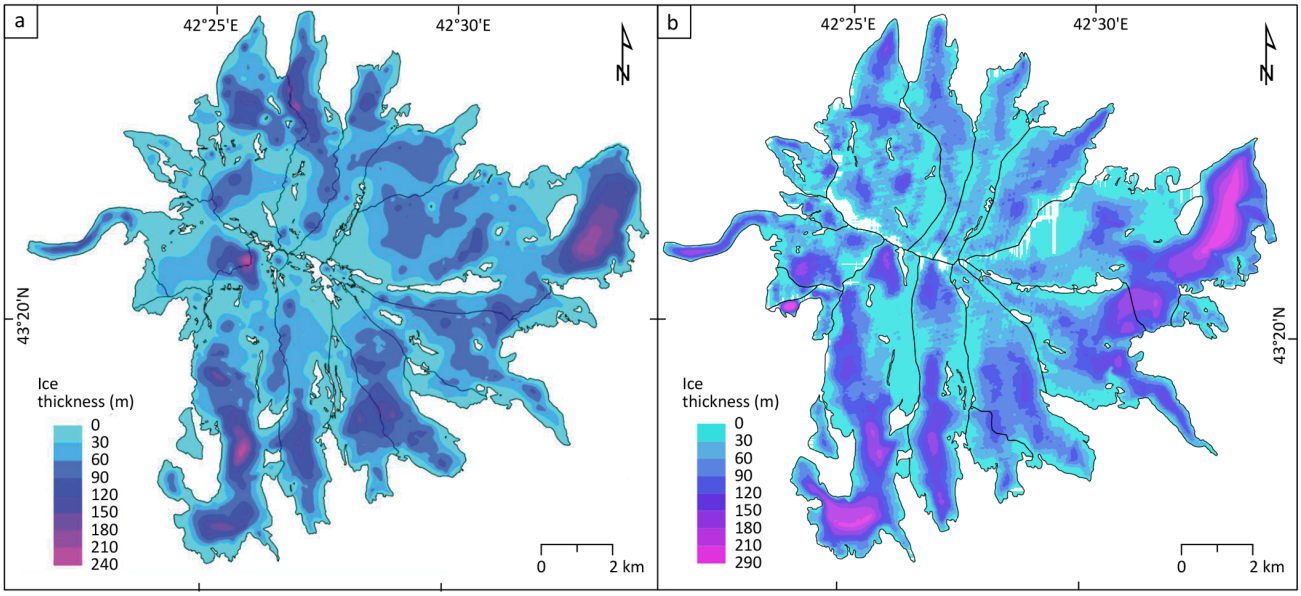


Figure 10. Comparison of glacier thickness across the Elbrus glacier system. (**a**) 2017 (Kutuzov et al., 2019) [33] and (**b**) 2014 (this study).

Overall, the close agreement between the two datasets provides independent support for the reconstructed glacier evolution, while differences in absolute values likely reflect differences in inventory dates, glacier outlines, and ice-thickness methodologies.

5.4. Consistency Between Reconstructed Glacier Volume Changes and Regional Geodetic Mass Balance

To facilitate comparison with independent glacier mass-balance observations, the reconstructed glacier volume changes were converted to specific mass changes expressed in metres water equivalent (m w.e.). Following the approach of Dussaillant et al. (2025) [10], a glacier ice density of 850 ± 60 kg m^{-3} was applied to the reconstructed volume changes. For each observation interval, the volume change was normalized by the mean glacierized area of the corresponding period, providing an estimate of the regional mean specific mass change. The resulting cumulative mass-change series is compared with the regional WGMS-based record of Dussaillant et al. (2025) [10] in Figure 11.

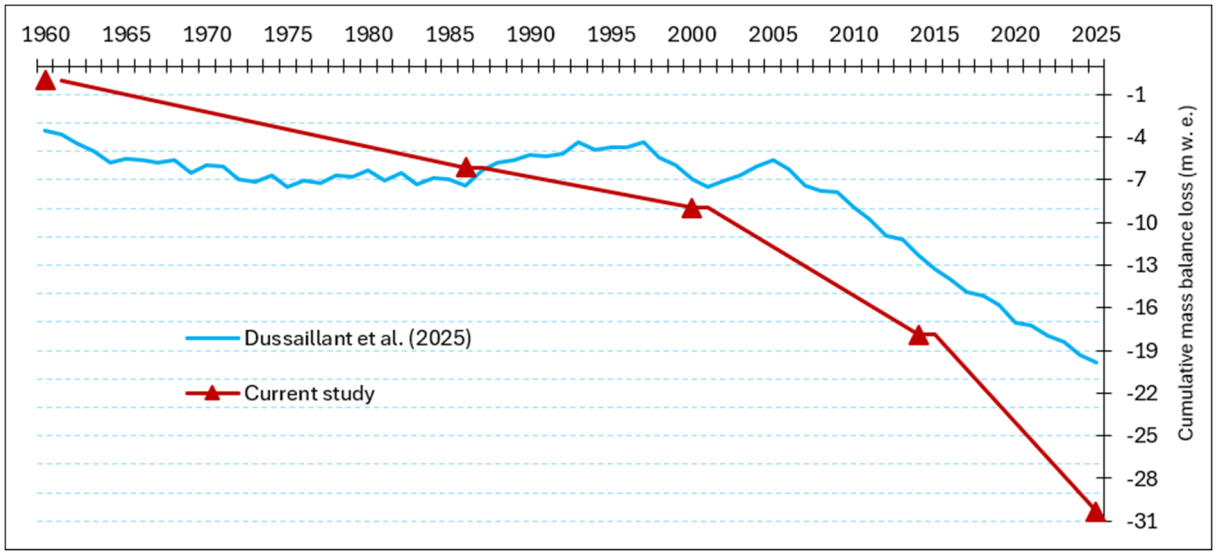


Figure 11. Comparison of cumulative glacier mass change derived from reconstructed glacier volume changes and the WGMS-based regional mass-balance record of Dussaillant et al. (2025) [10]. Mass changes are expressed in metres water equivalent (m w.e.).

The volume-derived mass-balance estimates indicate a progressive acceleration of glacier mass loss across the Greater Caucasus. The mean annual mass change was approximately -0.23 m w.e. yr^{-1} during 1960–1986 and -0.20 m w.e. yr^{-1} during 1986–2000, increasing to -0.64 m w.e. yr^{-1} during 2000–2014 and -1.13 m w.e. yr^{-1} during 2014–2025. Over the full 1960–2025 period, the reconstructed volume loss corresponds to a cumulative mass change of approximately -30.3 m w.e. These results indicate a marked increase in the rate of ice loss after 2000, with the strongest volume-derived mass loss occurring during the most recent observation interval.

The acceleration evident in both cumulative records is consistent with recent regional and global assessments documenting increasingly negative glacier mass balances during the twenty-first century [9,10,35]. This acceleration of ice loss corresponds to a period when global warming has accelerated markedly [79]. Atmospheric warming has intensified glacier mass losses throughout many mountain regions, including the Greater Caucasus [80]. The increasingly steep gradients of both curves after 2000 suggest that glacier thinning has become progressively more widespread and that the rate of ice depletion has increased substantially during recent decades. This temporal agreement reinforces the interpretation that the pronounced glacier volume losses reconstructed in this study primarily reflect sustained climatic forcing rather than methodological artefacts.

6. Conclusions

This study presents the first regional-scale reconstruction of glacier volume evolution for the entire Greater Caucasus from 1960 to 2025. By combining multi-temporal glacier inventories with the automated PalaeoIce reconstruction framework, glacier centrelines derived from OGGM, and a reconstructed bare-earth digital elevation model, we quantified changes in glacier ice storage across five observation periods. Comparison with the independent IceBoost ice-volume dataset and regional geodetic mass-balance observations demonstrates that the reconstructed glacier volumes are both internally consistent and physically realistic, providing confidence in the long-term reconstruction.

The reconstructed glacier volumes indicate that total glacier storage declined from 88.08 $\pm$ 4.4 km^3 in 1960 to 42.66 $\pm$ 1.1 km^3 in 2025, representing an overall reduction of approximately 51.6% during the 65-year study period. Glacier shrinkage occurred throughout the observation period but accelerated markedly after 2000, with the most rapid losses recorded during 2014–2025.

Distinct spatial differences were identified across both political and physiographic subdivisions of the mountain range. Russia retained the largest absolute glacier reserves throughout the study period, whereas glaciers in Azerbaijan experienced the greatest proportional reductions, reflecting their limited ice reserves and greater climatic sensitivity. Similarly, the eastern Greater Caucasus exhibited the strongest relative losses during the early twenty-first century, while the western sector underwent the most rapid acceleration during the most recent observation interval. These patterns highlight the influence of regional climatic gradients, glacier size, and topographic setting on glacier response to ongoing atmospheric warming.

The comparison between glacier area and volume further demonstrates that changes in glacier extent alone do not adequately represent the magnitude of contemporary glacier change. While glacier outlines continue to provide essential information on glacier distribution, reconstructed ice volume, despite uncertainties associated with ice thickness estimates, offers a more comprehensive assessment of remaining freshwater storage because it incorporates both horizontal retreat and widespread glacier thinning.

Beyond providing a long-term regional assessment of glacier volume evolution in the Greater Caucasus, this study establishes an important quantitative baseline for future investigations of glacier dynamics, regional hydrology, natural hazards, and climate-change impacts. The methodology presented here also demonstrates the potential of using automated reconstruction approaches to estimate consistent multi-decadal glacier volumes in mountain regions where direct measurements of ice thickness remain scarce.

Author Contributions: Conceptualization, L.G.T. and Y.L.; methodology, L.G.T. and Y.L.; writing—original draft preparation, L.G.T. and Y.L.; writing—review and editing, L.G.T., Y.L., R.M.K., W.Y. and A.N.M.; visualization, L.G.T. and Y.L. All authors have read and agreed to the published version of the manuscript.

Funding: This work was supported by the Shota Rustaveli National Science Foundation of Georgia (SRNSFG; grant no FR-23-4258).

Data Availability Statement: The original contributions presented in this study are included in the article. Further inquiries can be directed to the corresponding author.

Acknowledgments: We thank Gennady Nosenko for his insightful comments during the preparation of this manuscript. We also thank the three anonymous reviewers for their insightful comments, which helped significantly improve the manuscript.

Conflicts of Interest: The authors declare no conflicts of interest.

References

1. Oerlemans, J. Quantifying Global Warming from the Retreat of Glaciers. *Science* **1994**, *264*, 243–245. [CrossRef] [PubMed]
2. Hock, R.; Rasul, G.; Adler, C.; Cáceres, B.; Gruber, S.; Hirabayashi, Y.; Jackson, M.; Kääb, A.; Kang, S.; Kutuzov, S.; et al. High Mountain Areas. In *IPCC Special Report on the Ocean and Cryosphere in a Changing Climate*; Pörtner, H.O., Roberts, D.C., Masson-Delmotte, V., Zhai, P., Tignor, M., Poloczanska, E., Mintenbeck, K., Alegría, A., Nicolai, M., Okem, A., et al., Eds.; Cambridge University Press: Cambridge, UK; New York, NY, USA, 2019.
3. Marzeion, B.; Cogley, J.G.; Richter, K.; Parkes, D. Attribution of global glacier mass loss to anthropogenic and natural causes. *Science* **2014**, *345*, 919–921. [CrossRef] [PubMed]
4. Zekollari, H.; Schuster, L.; Maussion, F.; Hock, R.; Marzeion, B.; Rounce, D.R.; Compagno, L.; Fujita, K.; Huss, M.; James, M.; et al. Glacier preservation doubled by limiting warming to 1.5 °C versus 2.7 °C. *Science* **2025**, *388*, 979–983. [CrossRef] [PubMed]
5. Huss, M.; Bookhagen, B.; Huggel, C.; Jacobsen, D.; Bradley, R.S.; Clague, J.J.; Vuille, M.; Buytaert, W.; Cayan, D.R.; Greenwood, G.; et al. Toward mountains without permanent snow and ice. *Earth's Future* **2017**, *5*, 418–435. [CrossRef]
6. Huss, M.; Hock, R. Global-scale hydrological response to future glacier mass loss. *Nat. Clim. Change* **2018**, *8*, 135–140. [CrossRef]
7. Hock, R.; Truffer, M. Glacier hazards: Will they change in the future? *Arct. Antarct. Alp. Res.* **2024**, *56*, 2335991. [CrossRef]
8. GlaMBIE Team. Community estimate of global glacier mass changes from 2000 to 2023. *Nature* **2025**, *639*, 382–388. [CrossRef] [PubMed]
9. Hugonnet, R.; McNabb, R.; Berthier, E.; Menounos, B.; Nuth, C.; Girod, L.; Farinotti, D.; Huss, M.; Dussaillant, I.; Brun, F.; et al. Accelerated global glacier mass loss in the early twenty-first century. *Nature* **2021**, *592*, 726–731. [CrossRef] [PubMed]
10. Dussaillant, I.; Hugonnet, R.; Huss, M.; Berthier, E.; Bannwart, J.; Paul, F.; Zemp, M. Annual mass change of the world's glaciers from 1976 to 2024 by temporal downscaling of satellite data with in situ ob-servations. *Earth Syst. Sci. Data* **2025**, *17*, 1977–2006. [CrossRef]
11. The WGMS Network. Global glacier mass change in 2025. *Nat. Rev. Earth Environ.* **2026**, *7*, 213–215. [CrossRef]
12. Vargo, L.J.; Anderson, B.M.; Dadić, R.; Horgan, H.J.; Mackintosh, A.N.; King, A.D.; Lorrey, A.M. Anthropogenic warming forces extreme annual glacier mass loss. *Nat. Clim. Change* **2020**, *10*, 856–861. [CrossRef]
13. Salerno, F.; Guyennon, N.; Yang, K.; Shaw, T.E.; Lin, C.; Colombo, N.; Romano, E.; Gruber, S.; Bolch, T.; Alessandri, A.; et al. Local cooling and drying induced by Himalayan glaciers under global warming. *Nat. Geosci.* **2023**, *16*, 1120–1127. [CrossRef]
14. Ren, S.; Jia, L.; Miles, E.S.; Menenti, M.; Kneib, M.; Shaw, T.E.; Buri, P.; McCarthy, M.J.; Yang, W.; Pellicciotti, F.; et al. Observed and projected declines in glacier albedo across the Third Pole in the 21st century. *One Earth* **2024**, *7*, 1587–1599. [CrossRef]
15. Zhou, J.; Sun, W.; Huai, B.; Wang, Y.; An, H.; Chen, R.; Han, C.; Wang, L. Glacier induced different changing patterns of temperature and precipitation on glacial regions compared with nonglacial regions over Tibetan Plateau. *Atmos. Res.* **2026**, *330*, 108576. [CrossRef]
16. Zemp, M.; Jakob, L.; Brun, F.; Sutterley, T.; Menounos, B. Glacier monitoring from space is crucial, and at risk. *Eos* **2025**, *106*. [CrossRef]
17. Wouters, B.; Gardner, A.S.; Moholdt, G. Global glacier mass loss during the GRACE satellite mission (2002–2016). *Front. Earth Sci.* **2019**, *7*, 96. [CrossRef]
18. Berthier, E.; Floriciou, D.; Gardner, A.S.; Gourmelen, N.; Jakob, L.; Paul, F.; Treichler, D.; Wouters, B.; Belart, J.M.C.; Dehecq, A.; et al. Measuring glacier mass changes from space—A review. *Rep. Prog. Phys.* **2023**, *86*, 036801. [CrossRef] [PubMed]
19. Thongley, T.; Tielidze, L.G.; Yang, W.; Gunn, A.; Mackintosh, A.N. Accelerated Glacier Area Loss and Extinction of Small Glaciers in the Bhutanese Himalaya over the Past Five Decades. *Remote Sens.* **2026**, *18*, 323. [CrossRef]
20. Forte, E.; Gutgesell, P.; Securo, A.; Marcer, M.; Citterio, M.; Machguth, H.; Colucci, R.R. Comparing GPR with ice thickness and thermal models: Insights from two polythermal glaciers in West Greenland. *J. Glaciol.* **2025**, *71*, e97. [CrossRef]
21. Vergnano, A.; Franco, D.; Godio, A. Integrating GPR and ice-thickness models for improved bedrock detection: The case study of Rutor temperate glacier. *Cryosphere* **2025**, *19*, 6965–6988. [CrossRef]
22. Bamber, J.L.; Rivera, A. A review of remote sensing methods for glacier mass balance determination. *Glob. Planet. Change* **2007**, *59*, 138–148. [CrossRef]
23. Van Wyk de Vries, M.; Carchipulla-Morales, D.; Wickert, A.D.; Minaya, V.G. Glacier thickness and ice volume of the Northern Andes. *Sci. Data* **2022**, *9*, 342. [CrossRef]
24. Maffezzoli, N.; Rignot, E.; Barbante, C.; Morlighem, M.; Petersen, T.C.; Vascon, S. Machine-learned global glacier ice volumes. *Sci. Data* **2026**, *13*, 1104. [CrossRef] [PubMed]
25. Reinthaler, J.; Paul, F. Reconstructed glacier area and volume changes in the European Alps since the Little Ice Age. *Cryosphere* **2025**, *19*, 753–767. [CrossRef]
26. Marzeion, B.; Champollion, N.; Haeberli, W.; Langley, K.; Leclercq, P.; Paul, F. Observation-Based Estimates of Global Glacier Mass Change and Its Contribution to Sea-Level Change. *Surv. Geophys.* **2017**, *38*, 105–130. [CrossRef] [PubMed] [PubMed Central]

27. Zekollari, H.; Huss, M.; Schuster, L.; Maussion, F.; Rounce, D.R.; Aguayo, R.; Champollion, N.; Compagno, L.; Hugonnet, R.; Marzeion, B.; et al. Twenty-first century global glacier evolution under CMIP6 scenarios and the role of glacier-specific observations. *Cryosphere* **2024**, *18*, 5045–5066. [CrossRef]
28. Mackay, J.D.; Barrand, N.E.; Hannah, D.M.; Potter, E.; Montoya, N.; Buytaert, W. Physically based modelling of glacier evolution under climate change in the tropical Andes. *Cryosphere* **2025**, *19*, 685–712. [CrossRef]
29. Jomelli, V.; Tielidze, L.G.; Charton, J.; Mackintosh, A.N.; Elashvili, M.; Acuña Reyes, N.; Nadaraia, A.; Aumaitre, G.; Keddadouche, K.; Zaidi, F. Glaciers fluctuations during the Lateglacial and the Holocene in Georgian Greater Caucasus from 10Be moraine dating. *Holocene* **2026**, 1–15. [CrossRef]
30. Shahgedanova, M.; Nosenko, G.; Kutuzov, S.; Rototaeva, O.; Khromova, T. Deglaciation of the Caucasus Mountains, Russia/Georgia, in the 21st century observed with ASTER satellite imagery and aerial photography. *Cryosphere* **2014**, *8*, 2367–2379. [CrossRef]
31. Tielidze, L.G. Glacier change over the last century, Caucasus Mountains, Georgia, observed from old topographical maps, Landsat and ASTER satellite imagery. *Cryosphere* **2016**, *10*, 713–725. [CrossRef]
32. Tielidze, L.G.; Wheate, R.D. The Greater Caucasus Glacier Inventory (Russia, Georgia and Azerbaijan). *Cryosphere* **2018**, *12*, 81–94. [CrossRef]
33. Kutuzov, S.; Lavrentiev, I.; Smirnov, A.; Nosenko, G.; Petrakov, D. Volume Changes of Elbrus Glaciers From 1997 to 2017. *Front. Earth Sci.* **2019**, *7*, 153. [CrossRef]
34. Tielidze, L.G.; Nosenko, G.A.; Khromova, T.E.; Paul, F. Strong acceleration of glacier area loss in the Greater Caucasus between 2000 and 2020. *Cryosphere* **2022**, *16*, 489–504. [CrossRef]
35. Tielidze, L.G.; Jomelli, V.; Nosenko, G.A. Analysis of Regional Changes in Geodetic Mass Bal-ance for All Caucasus Glaciers over the Past Two Decades. *Atmosphere* **2022**, *13*, 256. [CrossRef]
36. Tielidze, L.G.; Nosenko, G.A.; Nadaraia, A.; Khromova, T.E.; Kumladze, R.M.; Clason, C.C.; Elashvili, M.; Gadrani, L. A 2025 High-Resolution Glacier Inventory of the Greater Caucasus Reveals Accelerated Area Loss. *Remote Sens.* **2026**, *18*, 1441. [CrossRef]
37. Li, Y. PalaeoIce: An automated method to reconstruct palaeoglaciers using geomorphic evidence and digital elevation models. *Geomorphology* **2023**, *421*, 108523. [CrossRef]
38. Chen, X.; Yang, W.; Li, Y.; Yang, Y.; Liu, J.; Liu, Q. Timing and extent of glacial fluctuations around Mt. Noijin Kangsang on the southern Tibetan Plateau during the Little Ice Age. *Palaeogeogr. Palaeoclimatol. Palaeoecol.* **2024**, *640*, 112092. [CrossRef]
39. Glasser, N.F.; Harrison, S.; Wilson, R.; Wood, J.; Peacey, M.; Rood, D.; Nichols, K.; Colucci, R.R.; Del Gobbo, C.; Securo, A.; et al. Younger Dryas glacier advances in the tropical Andes driven by increased precipitation. *Sci. Rep.* **2025**, *15*, 30832. [CrossRef] [PubMed]
40. Delmas, M.; Reixach, T.; Braucher, R.; Girault, I.; Torcheboeuf, M.E.; Gunnell, Y.; Calvet, M.; Pétillon, J.M. Multi-method constraints on late Pleistocene glacier fluctuations in the Ossau valley (SW France). with wider implications for the Pyrenean icefield during the last glacial maximum. *Quat. Sci. Rev.* **2026**, *378*, 109880. [CrossRef]
41. Mikhalenko, V.; Sokratov, S.; Kutuzov, S.; Ginot, P.; Legrand, M.; Preunkert, S.; Lavrentiev, I.; Kozachek, A.; Ekaykin, A.; Faïn, X.; et al. Investigation of a deep ice core from the Elbrus western plateau, the Caucasus, Russia. *Cryosphere* **2015**, *9*, 2253–2270. [CrossRef]
42. Forte, A.M.; Whipple, K.X.; Bookhagen, B.; Rossi, M.W. Decoupling of modern shortening rates, climate, and topography in the Caucasus. *Earth Planet. Sci. Lett.* **2016**, *449*, 282–294. [CrossRef]
43. Kaftan, V.I.; Gvishiani, A.D.; Manevich, A.I.; Dzeboev, B.A.; Tatarinov, V.N.; Dzeranov, B.V.; Avdonina, A.M.; Losev, I.V. An Analytical Review of the Recent Crustal Uplifts, Tectonics, and Seismicity of the Caucasus Region. *Geosciences* **2024**, *14*, 70. [CrossRef]
44. Volodicheva, N. The Caucasus. In *The Physical Geography of Northern Eurasia*; Shahgedanova, M., Ed.; Oxford University Press: Oxford, UK, 2002; pp. 350–376.
45. Tielidze, L.G.; Iacob, G.; Holobâcă, I.H. Mapping of Supra-Glacial Debris Cover in the Greater Caucasus: A Semi-Automated Multi-Sensor Approach. *Geosciences* **2024**, *14*, 178. [CrossRef]
46. Tielidze, L.G.; Mackintosh, A.N.; Gavashelishvili, A.; Gadrani, L.; Nadaraia, A.; Elashvili, M. Post-Little Ice Age Equilibrium-Line Altitude and Temperature Changes in the Greater Caucasus Based on Small Glaciers. *Remote Sens.* **2025**, *17*, 1486. [CrossRef]
47. Nye, J.F. A Method of Calculating the Thicknesses of the Ice-Sheets. *Nature* **1952**, *169*, 529–530. [CrossRef]
48. Benn, D.I.; Hulton, N.R.J. An Excel (TM) spreadsheet program for reconstructing the surface profile of former mountain glaciers and ice caps. *Comput. Geosci.* **2010**, *36*, 605–610. [CrossRef]
49. Glen, J.W. W.S.B. Paterson 1994. The physics of glaciers. 3rd edition. Oxford, etc., Pergamon, 480 pp. ISBN 0-08037945 1. Hardback. £70; 0-O8O37944 3, Flexieover. £25. *J. Glaciol.* **1997**, *43*, 594. [CrossRef]
50. Nye, J.F. The Mechanics of Glacier Flow. *J. Glaciol.* **1952**, *2*, 82–93. [CrossRef]
51. Schilling, D.H.; Hollin, J.T. Numerical reconstructions of valley glaciers and small ice caps. In *The Last Great Ice Sheets*; Denton, G.H., Hughes, T.J., Eds.; Wiley: New York, NY, USA, 1981; pp. 207–220.

52. Van der Veen, C.J. *Fundamentals of Glacier Dynamics*; Balkema: Rotterdam, The Netherlands, 1999; p. 462.
53. Khandsuren, P.; Seong, Y.B.; Rhee, H.H.; Demberel, O.; Yu, B.Y. Glacial chronology and topographic controls in the Tsambagarav Massif, western Mongolia: Insights from 10Be dating. *Quat. Sci. Rev.* **2026**, *376*, 109817. [CrossRef]
54. Larocca, L.J.; Kaufman, D.S.; Erb, M.P.; Schultz, T.M.; McKay, N.P.; Brooks, J.P.; Carrivick, J.L. Glacier Equilibrium-Line Altitude Change Across Alaska and Adjacent Canada Indicates a Cold, Dry Little Ice Age and Weaker Aleutian Low. *Geophys. Res. Lett.* **2026**, *53*, e2025GL119840. [CrossRef]
55. Leontaritis, A.D.; Moraetis, D.; Pavlopoulos, K.; Hughes, P.D.; Fassoulas, C. Quaternary Glaciation in the Mountains of Crete, Greece. *Quat. Sci. Rev.* **2025**, *369*, 109598. [CrossRef]
56. Lin, S.; Liu, J.; Li, Y.; Hu, H.; Ye, C.; Liu, Q.; Pi, S. Glacial changes in the eastern Kunlun Mountains since the Little Ice Age. *Quat. Int.* **2026**, *753*, 110053. [CrossRef]
57. Sun, Y.; Xu, X.; Zhang, H.; Li, J. Reconstructions of global last glacial maximum glaciers and climate in the Karakoram Mountains, northwestern Tibetan plateau. *CATENA* **2026**, *265*, 109900. [CrossRef]
58. Sun, Y.; Xu, X.; Zhang, H.; Li, J.; Xu, B. Can inter-annual climate variability alone explain the glacier retreat since the Little Ice Age in the Hailuogou catchment, southeastern Tibetan Plateau? *Palaeogeogr. Palaeoclimatol. Palaeoecol.* **2024**, *638*, 112039. [CrossRef]
59. Ventura, J.; Oliva, M.; Fernández-Fernández, J.M.; Fernandes, M.; Palacios, D.; Leger, T.; Jomelli, V.; Grau, O.; ASTER Team. Glacial and periglacial dynamics during the last deglaciation in the Bonabé Valley (Marimanha Massif), central southern Pyrenees. *Geomorphology* **2025**, *482*, 109801. [CrossRef]
60. Yang, Y.; Yang, W.; Li, Y.; Liu, F.; Xiao, J.; Liu, B.; Li, M.; Liu, G. Reconstruction of palaeoglaciers and palaeoclimate in Zheduo Shan, Eastern Tibetan Plateau, during the Last Glacial Maximum. *Quat. Int.* **2023**, *673*, 18–28. [CrossRef]
61. Zhang, H.; Xu, X.; Li, Y.; Sun, Y.; Xu, B.; Li, J. Glacier mass loss on the southeastern Tibetan Plateau since the Little Ice Age. *J. Quat. Sci.* **2025**, *40*, 807–819. [CrossRef]
62. Zhang, H.-J.; Xu, X.-K.; Li, Y.-K.; Liu, L.; Sun, Y.-Q.; Li, J.-L. Changes in glaciers and climate in the Karakoram since the little ice age. *Adv. Clim. Change Res.* **2026**, *17*, 780–794. [CrossRef]
63. Maussion, F.; Butenko, A.; Champollion, N.; Dusch, M.; Eis, J.; Fourteau, K.; Gregor, P.; Jarosch, A.H.; Landmann, J.; Oesterle, F. The Open Global Glacier Model (OGGM) v1.1. *Geosci. Model Dev.* **2019**, *12*, 909–931. [CrossRef]
64. Kienholz, C.; Rich, J.L.; Arendt, A.A.; Hock, R. A new method for deriving glacier centerlines applied to glaciers in Alaska and northwest Canada. *Cryosphere* **2014**, *8*, 503–519. [CrossRef]
65. RGI 7.0 Consortium. *Randolph Glacier Inventory—A Dataset of Global Glacier Outlines, Version 7.0.*; NSIDC: National Snow and Ice Data Center: Boulder, CO, USA, 2023. [CrossRef]
66. James, W.H.M.; Carrivick, J.L. Automated modelling of spatially-distributed glacier ice thickness and volume. *Comput. Geosci.* **2016**, *92*, 90–103. [CrossRef]
67. Zhao, X.; Zhao, Z.; Liu, J.; Liu, Q.; Li, Y. Influences of multi-source and multi-resolution DEMs on glacier simulation in Mt.NoijinKangsang. *Quat. Sci.* **2022**, *42*, 1181–1192. (In Chinese)
68. Farinotti, D.; Huss, M.; Fürst, J.J.; Landmann, J.; Machguth, H.; Maussion, F.; Pandit, A. A consensus estimate for the ice thickness distribution of all glaciers on Earth. *Nat. Geosci.* **2019**, *12*, 168–173. [CrossRef]
69. Millan, R.; Mouginot, J.; Rabatel, A.; Morlighem, M. Ice velocity and thickness of the world's glaciers. *Nat. Geosci.* **2022**, *15*, 124–129. Correction in *Nat. Geosci.* **2023**, *16*, 188. [CrossRef]
70. Zhang, H.; Xu, X.; Sun, Y.; Li, J.; Xu, B. Reconstructions of Little Ice Age glaciers and climate in the Tanggula Mountains, Central Tibet Plateau. *Palaeogeogr. Palaeoclimatol. Palaeoecol.* **2024**, *637*, 112008. [CrossRef]
71. Tuszynski, J. caTools: Tools: Moving Window Statistics, GIF, Base64, ROC AUC, Etc. R Package Version: 1.10. 2009. Available online: http://CRAN.R-project.org/package=caTools (accessed on 27 August 2026).
72. Rototaeva, O.V.; Nosenko, G.A.; Kerimov, A.M.; Kutuzov, S.S.; Lavrentiev, I.I.; Nikitin, S.A.; Kerimov, A.A.; Tarasova, L.N. Changes of the mass balance of the Garabashy Glacier, Mount Elbrus, at the turn of 20th and 21st centuries. *Ice Snow* **2019**, *59*, 5–22. [CrossRef]
73. Tielidze, L.G.; Svanadze, D.; Gadrani, L.; Asanidze, L.; Wheate, R.D.; Hamilton, G.S. A 54-year record of changes at Chalaati and Zopkhito glaciers, Georgian Caucasus, observed from archival maps, satellite imagery, drone survey and ground-based investigation. *Hung. Geogr. Bull.* **2020**, *69*, 175–189. [CrossRef]
74. Bahr, D.B.; Pfeffer, W.T.; Sassolas, C.; Meier, M.F. Response time of glaciers as a function of size and mass balance: 1. *Theory. J. Geophys. Res.* **1998**, *103*, 9777–9782. [CrossRef]
75. Mackintosh, A.N.; Anderson, B.M.; Pierrehumbert, R.T. Reconstructing climate from glaciers. *Annu. Rev. Earth Planet. Sci.* **2017**, *45*, 649–680. [CrossRef]
76. Bosson, J.-B.; Huss, M.; Osipova, E. Disappearing World Heritage glaciers as a keystone of nature conservation in a changing climate. *Earth's Future* **2019**, *7*, 469–479. [CrossRef]
77. Van Tricht, L.; Zekollari, H.; Huss, M.; Rounce, D.R.; Schuster, L.; Aguayo, R.; Schmitt, P.; Maussion, F.; Tober, B.; Farinotti, D. Peak glacier extinction in the mid-twenty-first century. *Nat. Clim. Change* **2026**, *16*, 143–147. [CrossRef] [PubMed]

78. Sommer, C.; Malz, P.; Seehaus, T.C.; Lippl, S.; Zemp, M.; Braun, M.H. Rapid glacier retreat and downwasting throughout the European Alps in the early 21st century. *Nat. Commun.* **2020**, *11*, 3209. [CrossRef] [PubMed]
79. Foster, G.; Rahmstorf, S. Global warming has accelerated significantly. *Geophys. Res. Lett.* **2026**, *53*, e2025GL118804. [CrossRef]
80. Toropov, P.A.; Aleshina, M.A.; Grachev, A.M. Large-scale climatic factors driving recession in the Greater Caucasus, 20th–21st century. *Int. J. Climatol.* **2019**, *39*, 4703–4720. Correction in *Int. J. Climatol.* **2020**, *40*, 1928–1930. [CrossRef]

Disclaimer/Publisher's Note: The statements, opinions and data contained in all publications are solely those of the individual author(s) and contributor(s) and not of MDPI and/or the editor(s). MDPI and/or the editor(s) disclaim responsibility for any injury to people or property resulting from any ideas, methods, instructions or products referred to in the content.